SEPAC DATA ANALYSIS IN SUPPORT OF THE ENVIRONMENTAL INTERACTION PROGRAM

by

C. S. Lin

FINAL TECHNICAL REPORT

NASA Contract NAS8-32488, Task 4

SwRI Project 15-4865-009

Prepared for

National Aeronautics and Space Administration

George C. Marshall Space Flight Center

Marshall Space Flight Center, Alabama 35812

March 31, 1991

NASA

Report Documentation Page

1. Report No	2. Government Accession No.	3. Recipient's Catalog No.

4. Title and Subtitle
Participation in the Definition, Conduct, and Analysis of Particle Accelerator Experiments for the First Spacelab Mission

5. Report Date
April 1991

6. Performing Organization Code

7. Author(s)
Chin S. Lin

8. Performing Organization Report No.
15-4865-009

10. Work Unit No.

9. Performing Organization Name and Address

11. Contract or Grant No.
NAS8-32488 (Task 4)

13. Type of Report and Period Covered
Final Report
Nov. 1987 - April 1991

12. Sponsoring Agency Name and Address
National Aeronautics and Space Administration
George C. Marshall Space Flight Center
Marshall Space Flight Center, Alabama 35812

14. Sponsoring Agency Code

15. Supplementary Notes

16. Abstract

This report summarizes the research findings obtained during the support of the NASA Contract NAS8-32488 Task 4. The objective of the project is to conduct data analyses of SEPAC data and computer modeling to investigate spacecraft environmental effects associated with injection of electron beams, plasma clouds and neutral gas clouds from the Shuttle orbiter. The data analysis indicates that ELF oscillations from 150 to 200 Hz were seen in the Langmuir probe current when the beam was fired in a continuous mode. The strongest oscillations occurred when the ambient pressure was augmented by neutral gas releases from the SEPAC plasma accelerator MPD. To understand the dependence of spacecraft charging potential on beam density and other plasma parameters, we have used a two-dimensional electrostatic particle code to simulate the injection of electron beams from an infinite conductor into a plasma. The simulations show that the conductor charging potential depends critically on the reflection coefficient of the conductor surface, which is defined as the percentage of incident particles reflected by the conductor. The ionization effects on spacecraft charging are examined by including interactions of electrons with neutral gas. The simulations show that the conductor charging potential decreases with increasing neutral background density

(continued)

17. Key Words (Suggested by Author(s))	18. Distribution Statement
spacecraft charging potential electron beam injection neutral gas ionization	Unclassified--Unlimited

19. Security Classif. (of this report)	20. Security Classif. (of this page)	21. No. of pages	22. Price

Block 16 continuation

due to the production of secondary electrons near the conductor surface. The simulations also indicate that the beam radius is generally proportional to the beam electron gyroradius when the conductor is charged to a large potential. It appears that the charge buildup at the beam stagnation point causes the beam radial expansion. A survey of the simulation results suggests that the ratio of the beam radius to the beam electron gyroradius increases with the square root of beam density and decreases inversely with beam injection velocity. These results are useful for explaining the spacecraft charging phenomena observed during SEPAC experiments from Spacelab 1.

Southwest Research Institute
Post Office Drawer 28510, 6220 Culebra Road
San Antonio, Texas 78284

SEPAC DATA ANALYSIS IN SUPPORT OF THE ENVIRONMENTAL INTERACTION PROGRAM

by
C. S. Lin

FINAL TECHNICAL REPORT
NASA Contract NAS8-32488, Task 4
SwRI Project 15-4865-009

Prepared for
National Aeronautics and Space Administration
George C. Marshall Space Flight Center
Marshall Space Flight Center, Alabama 35812

March 31, 1991

Approved:

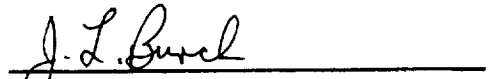

James L. Burch, Vice President
Instrumentation and Space Research

Table of Contents

I INTRODUCTION

This report summarizes the research findings obtained during the support of the NASA Contract NAS8-32488 Task 4. The objective of the project is to conduct data analyses of SEPAC data and computer modeling to investigate spacecraft environmental effects associated with injection of electron beams, plasma clouds and neutral gas clouds from the Shuttle orbiter. Through this project, we participated in the development of spacecraft plasma interaction models in support of the NASA Lewis Research Center's Environmental Interaction Program. This final report summarizes the results from large-scale particle-in-cell simulations of interactions of Space Shuttle-generated electron beams with ambient plasma above the Earth's ionosphere.

High current energetic electron beams have been injected from the Spacelab-1 payload using the Space Experiments with Particle Accelerators (SEPAC) instrumentation to study the interactions of electron beams with ambient plasma. The SEPAC experiments indicate that the electron beam injection had charged the spacecraft to a potential as high as the beam energy. Analysis of the SEPAC data suggests that spacecraft charging during beam emissions into a plasma is a complicated function of beam energy, ambient plasma density, Shuttle velocity, locations of conducting surfaces, conductor surface property, and probably other unknown factors. Therefore, the simulation study conducted for this project has focused on the understanding of the spacecraft charging phenomenon. The results are applied to explain the spacecraft charging potential measured during the SEPAC experiments from Spacelab 1.

II SUMMARY OF RESEARCH RESULTS

Nonrelativistic electron beams have been injected from rockets and the Space shuttle to study beam propagation, instabilities and other space plasma problems in the ionosphere [Grandal, 1982]. Several experimental and theoretical studies have focused on the spacecraft charging phenomenon during the electron beam injection [Sasaki et al, 1986; Sasaki et al., 1987; Katz et al., 1986; Marshall et al., 1988]. At low beam current, Spacelab 2 experiments indicated that electron beams can propagate away after beam degradation and expansion [Gurnett et al., 1986]. However, at high beam current, Space Experiments with Particle Accelerators (SEPAC) during the Spacelab 1 mission indicated that the electron beam injection had charged the spacecraft to a potential as high as the beam energy, which was 5 keV [Sasaki et al., 1986]. Neutralization of spacecraft charging is therefore important for allowing the injected electron beam to propagate away. SEPAC experiments have suggested that a large conductor surface area for collecting currents from ambient plasma will reduce spacecraft charging.

We have completed four works related to spacecraft charging; we briefly summarize the results here and present the details in the next four sections.

A Spacecraft Charging Potential During Injection of an Electron Beam into Space Plasmas

Space Experiments with Particle Accelerators (SEPAC) during the Spacelab 1 mission indicated that the electron beam injection had charged the spacecraft to a potential as high as the beam energy, which was 5 keV. The charging potential increased linearly with the beam current for the beam current less than 100 mA and remained constant at about the beam energy for higher beam current. Since the electron beam energy was constant during the SEPAC experiments, the results imply that the charging potential is independent of the beam density for beam densities greater than a certain value.

Several simulation studies have examined the general relationship between the spacecraft charging and the electron beam injection in the ionosphere. All of these charging studies show that the positively charged spacecraft draws the ambient and the beam electrons to neutralize partially the charging. However, the SEPAC results, which indicate an empirical relationship between the charging potential and the beam density, have not been explained.

To understand the dependence of spacecraft charging potential on beam density and other plasma parameters, we have used a two-dimensional electrostatic particle code to simulate the injection of electron beams from an infinite conductor into a plasma. The simulations show that the conductor charging potential at the end of simulations does not vary with the beam density when the beam density exceeds four times the ambient density. The simulations

have modeled the effects of electron interactions with the conductor surface on the spacecraft charging. The surface either absorbs or reflects electrons impinging upon the surface. By examining how the conductor potential at the end of simulations varies with the simulation parameters, we found that the conductor charging potential depends critically on the reflection coefficient of the conductor surface, which is defined as the percentage of incident particles reflected by the conductor. To charge the conductor to the beam energy, the reflection coefficient needs to be about 0.5. The results are applied to explain the spacecraft charging potential measured during the SEPAC experiments from Spacelab 1. The simulation model and results are given in appendix A.

B Neutralization of Spacecraft Charging Potential by Neutral Gas Ionization

Injections of nonrelativistic electron beams from an isolated equipotential conductor into a uniform background of plasma and neutral gas have been simulated using a two-dimensional electrostatic particle code. The ionization effects on spacecraft charging are examined by including interactions of electrons with neutral gas. The simulations show that the conductor charging potential decreases with increasing neutral background density due to the production of secondary electrons near the conductor surface. In the spacecraft wake, the background electrons accelerated towards the charged spacecraft produce an enhancement of secondary electrons and ions. Simulations run for long duration indicate that the spacecraft potential is further reduced and short wavelength beam-plasma oscillations appear. These results are described in Section 3.

C Radial Expansion of an Injected Electron Beam

A two-dimensional electrostatic particle code has been used to study the beam radial expansion of a nonrelativistic electron beam injected from an isolated equipotential conductor into a background plasma. The simulations indicate that the beam radius is generally proportional to the beam electron gyroradius when the conductor is charged to a large potential. The simulations also suggest that the charge buildup at the beam stagnation point causes the beam radial expansion. From a survey of the simulation results, it is found that the ratio of the beam radius to the beam electron gyroradius increases with the square root of beam density and decreases inversely with beam injection velocity. This dependence is explained in terms of the ratio of the beam electron Debye length to the ambient electron Debye length. These results are described in Section 4.

D SEPAC Data Analysis

SEPAC (Space Experiments with Particle Accelerators) and PICPAB (Phenomena Induced by Charged Particle Beams) were part of the payload of Spacelab 1, which was flown onboard the Shuttle from November 28 through December 7, 1983. Both experiments contained particle accelerators as well as plasma diagnostics. One of the goals of SEPAC was to study the interaction of an energetic electron beam with the ambient plasma. The study presented here concerns observations of extremely low frequency (ELF) oscillations in data from the SEPAC diagnostic probes during firings of one of the PICPAB electron beams. These firings were sometimes coincident with releases of either plasma or neutral gas from one of the SEPAC accelerators: the magnetoplasma dynamic arcjet (MPD). Injections from an electron beam that comprised part of the PICPAB experiment were observed by the SEPAC plasma diagnostic package. In particular, ELF oscillations from 150 to 200 Hz were seen in the Langmuir probe current when the beam was fired in a continuous mode. The strongest oscillations occurred when the ambient pressure was augmented by neutral gas releases from the SEPAC plasma accelerator MPD.

Similar observations of ELF emissions during firings of the SEPAC electron beam were reported by Cai et al. [1987], who found oscillations < 500 Hz in data from the SEPAC Langmuir probes, floating probes, electron energy analyzer, and photometer. In that report a correlation was seen between the amplitude of the ELF oscillations and the charge-up potential of the orbiter, leading the authors to conclude that such oscillations are expressions of fluctuations in the return current (and hence spacecraft potential), caused by plasma processes occurring in the near environment. They propose that the oscillations may be electrostatic ion cyclotron waves generated close to the shuttle, possibly in a co-moving plasma cloud.

In this study we analyzed similar measurements with the same diagnostic package during firings of the electron beam from the PICPAB experiment. In all the cases studied, the 8-keV PICAB beam was fired at a current of 100 mA for a 20-ms pulse every 266 ms. Some of these firings occurred at times when the neutral pressure near the orbitor had been elevated above $7X10^{-5}$ by a release of neutral argon from one of the SEPAC plasma accelerators, the MPD. The technical report published in an IEEE journal is included as Appendix B.

III Neutralization of Spacecraft Charging Potential by Neutral Gas Ionization

A INTRODUCTION

It is well known that neutral gas ionization by the electron beam can help neutralize spacecraft charging. At altitudes below 160 km where neutral densities are high, electron beam experiments on sounding rockets indicate that payload charging was reduced and sometimes even completely neutralized [Szuszczewicz, 1985]. Plasma enhancement associated with Beam Plasma Discharge (BPD) [Papdopoulos and Szuszczewicz, 1989] is believed to be responsible for the charging neutralization of sounding rockets. During SEPAC electron beam experiments Marshall et al. [1988] reported anomalous features in the measurement of return current by Langmuir probe when an energetic electron beam was injected into a dense cloud of Argon gas. They interpreted the anomalous current signature as due to secondary electron fluxes escaping from the spacecraft and the formation of a double layer structure. In all cases of SEPAC experiments, the spacecraft potential charged by an electron beam was small relative to the beam energy when neutral gas was present.

The purpose of this work was to model the effects of neutral gas ionization on spacecraft charging due to electron beam injection. We used a two-dimensional electrostatic particle code to simulate the injection of electron beams from an isolated equipotential conductor into a uniform background of plasma and neutral gas. Specifically we examined how the spacecraft charging potential varies with neutral density.

Several simulation studies have examined the general relationship between the spacecraft charging and the electron beam injection in the ionosphere [Omura and Matsumoto, 1984; Pritchett and Winglee, 1987; Winglee and Pritchett, 1987; Okuda and Kan, 1987; Okuda and Berchem, 1988]. These studies show that the positively charged spacecraft attracts the ambient and beam electrons to neutralize the charging partially. Some electrons in the beam head, however, are accelerated forward and propagate away. Winglee and Prichett [1988] indicate that the spacecraft charging potential varies with the the injection angle of the beam relative to the magnetic field lines. Furthermore, the spacecraft charging potential exceeds the beam energy when the spacecraft surface is small relative to the return current region. Examining the surface effects of the spacecraft, Lin and Koga 1989] modeled the production of backscattered and secondary electrons generated at the conductor surface. Their simulations indicate that the spacecraft potential increases with the reflection coefficient, which is defined as the ratio of electrons reflected from the spacecraft surface.

B SIMULATION MODEL

To study electron beam injection from a conductor, we modified a 2-D particle-in-cell code DARWIN, which was originally developed at Los Alamos National Laboratory [Nelson and Lewis, 1976]. Here we present the simulation results in the electrostatic limit. We improve the modeling by considering (1) the injection of an electron beam from a finite isolated conductor and (2) collisional ionization of neutrals by beam, background, and secondary electrons. Figure 1 illustrates the simulation geometry.

We model the spacecraft as a rectangular conductor within the simulation system, which injects electrons from the spacecraft surface every timestep. The number of injected electrons per time step per cell is $N_c(n_b/n_c)v_b\Delta t$ where N_c is the number of ambient electrons per cell, Δt is the simulation time step, and n_b/n_c is the ratio of the beam density to background density. We assign the positions of the injected particles as $x = Rv_b\Delta t$ where x is the distance from the conductor surface, v_b is the injection velocity, and R is a random number between 0 and 1 for each injected particle. In the y direction we randomly distribute the injected particles across the beam. Therefore the injected particles fill in the fan between $x = 0$ and $x = v_b\Delta t$. In this study we assume that the spacecraft surface absorbs all particles striking the surface and accumulates the charge.

We use the capacity matrix method [Hockney and Eastwood, 1981] to treat the spacecraft surface as a finite isolated equipotential conductor in a background plasma. The capacity matrix C_{ij} relates the charge, q_i, on each grid point on the spacecraft to the corresponding potential Φ_j through

$$q_i = \sum_j C_{ij}\Phi_j \tag{1}$$

where the sum j is over every grid point on the spacecraft. The capacity matrix is obtained by placing a unit charge on one point of the spacecraft surface with all other points zero and then solving for the potential. The values of the potential at each point on the spacecraft represent one column in the inverse capacity matrix $A = C^{-1}$. Repeating the process for each node then generates the full inverse matrix. The capacity matrix is obtained from the inverse of this matrix. This process is carried out only once at the beginning of the program. During the program the code first solves Poisson's equation for the electric potential Φ_0 with the charge evenly distributed on the spacecraft surface. Second, it uses the capacity matrix of the conductor to redistribute the charge and maintain the spacecraft surface at an equipotential using the formulae:

$$\Delta q_i = \sum_j C_{ij}(\Phi_{eq} - \Phi_{0j}) \tag{2}$$

$$\Phi_{eq} = \sum_{ij} C_{ij}\Phi_{0j} / \sum_{ij} C_{ij} \tag{3}$$

where Δq_i is the charge that is added to each grid point on the spacecraft. Using the redistributed charge density, the code again solves Poisson's equation for the electric potential of the spacecraft.

We use a periodic boundary condition for the lower boundary at $y = 0$ and the upper boundary at $y = L_y$ where L_y is the simulation length in the y direction. The electrostatic potential at $x = 0$, $\phi(x = 0, y)$, is constant. We assume the potential is zero at the right boundary at $x = L_x$ where L_x is the simulation length in the x direction. The right boundary condition approximates the potential at the infinity.

In our model we include the interaction of beam, background, and secondary electrons with neutral particles following the approach of Machida and Goertz 1988]. The neutral particles are assumed uniformly distributed throughout the system. To allow the simulations to run for much longer times, a very high density neutral region is added at the right hand side of the simulation box. Beam electrons entering into this region are slowed down enough by collisions so that they are not reflected back into the simulation box with high velocities. All neutral particles are assumed to have a Maxwellian velocity distribution.

The ionization rate of the neutral particles is determined from the incoming electron velocity, the neutral density, and the ionization collisional cross section. The ionization collisional cross section varies with the incoming electron energy according to a fit to an experimental curve for O_2 [Banks and Kockarts, 1973]. We first calculate the ionization cross section based on the particle's energy and then calculate the average collisional ionization frequency from the cross section. Assuming that the event occurrence follows an exponential probability distribution, we assign a probability of collisional ionization P_i to the beam electrons at each time step. The probability is then compared with a uniform set of random numbers R_i between 0 and 1. A collision occurs if $P_i > R_i$.

A fixed ionization energy is subtracted from the incident particle energies after the collision. The velocity vectors of the electrons and ions after the collision are calculated from momentum conservation, energy conservation, and the assumption that the collisions are head on. Random directional angles are assigned to the particles after the collision. Other collisional processes can be handled in the same way as ionization collisions by using the appropriate collision frequency.

Background plasma ions and electrons are initialized uniformly in the system with a uniform magnetic field in the x direction. Both the background ions and electrons have Maxwellian velocity distributions with the same temperature, $T_e = T_i$ where T_e and T_i are the electron and ion temperatures, respectively. At the right and left boundary, the code specularly reflects all

particles.

C SIMULATION RESULTS

The simulation uses a $512\Delta \times 128\Delta$ grid in the x and y directions respectively. The spacecraft is represented by a rectangular box centered at $x = 102\Delta$ and $y = 64\Delta$ with size $4\Delta \times 32\Delta$ in the x and y directions respectively. The grid size, Δ, equals the Debye length of the ambient electrons defined as $\lambda_d = a_c/\omega_{pe}$ where $a_c = (2T_e/m_e)^{1/2}$ is the thermal velocity of the ambient electrons and ω_{pe} is the ambient electron plasma frequency. In the simulations $a_c = 0.001c$ where c is the speed of light, a unit of the simulation. We choose the secondary ion to electron mass ratio to be 1836. We assume the electron gyrofrequency Ω_{ce} to be $0.5\omega_{pe}$, which is close to the ionospheric value of $0.3\omega_{pe}$. The simulations use a time step $\Delta t = 0.05\omega_{pe}^{-1}$ and 131,072 particles for the background plasma. The electron beam has a width of 2Δ, an injection velocity of $v_b = 10a_c$, and zero thermal velocity. In this study, the density ratio n_b/n_o is 10 where n_b and n_o are the densities of the electron beam and the ambient electrons, respectively. In SEPAC experiments this ratio was approximately 100 for a 100 mA beam.

Figures 2 and 3 present the modeling results of an electron beam with no neutral background. The phase space plot at $\omega_{pe}t = 30$ indicates that the stagnation point of the injected electron beam is very close to the conductor surface (Figure 2a). Also it shows that beam electrons at the front are accelerated to velocities above the initial beam velocity, due to the buildup of beam electrons behind the front of the beam head. Figure 2b, the configuration space plot, shows that the electron beam expands radially due to mutual repulsion. The beam expands a maximum width of 40Δ near the spacecraft surface. Figure 3 shows the time variation of the spacecraft potential for the duration of the simulation. The oscillations in the potential correspond to the background plasma frequency. Note that after the quick rise in the potential to 75% of the beam energy the average potential is approximately 70% of the beam energy.

Figures 4-6 present results of an electron beam injected into a uniform background of neutral particles. The neutral number density is 10^{14} cm^{-3} corresponding to a pressure of 10^{-4} Torr at room temperature. The beam phase space plot at $\omega_{pe}t = 30$ in Figure 4a shows that the stagnation point of the beam is farther away from the spacecraft than the case with no neutral background. The beam electrons travel farther before being substantially slowed down because secondary electrons created from ionization of neutrals impinge on the spacecraft and reduce the charge. The configuration space plot in Figure 4b shows beam expansion similar to the case with no neutral background at $\omega_{pe}t = 30$. The maximum width remains at about 40Δ. The phase space plots of secondary electrons are shown in Figure 5. Figure 5a indicates that some secondary electrons near the spacecraft have been scattered to energies comparable to the beam energy. Most secondary electrons are produced

near the spacecraft surface while some are produced in the wake region of the spacecraft, as shown in the configuration space plot (Figure 5b). Secondary electrons are produced in the wake as background electrons are accelerated towards the charged spacecraft and ionize neutral particles. Figure 6 presents spacecraft potential as a function of time. The oscillations in the potential again correspond to the background plasma frequency. After a quick rise in the potential to 75% of the beam energy, the average potential energy of the spacecraft drops to about 40% of the beam energy. This reduction in the potential is caused by the increase in plasma density around the spacecraft from ionizations. Figure 7 shows spacecraft potential at $\omega_{pe}t = 30$ for various values of neutral density. This figure indicates that increasing the neutral density reduces the spacecraft potential. Two factors contribute to the reduction in the charging potential. First, higher neutral densities result in more collisional ionizations and therefore a larger number of secondary electrons to neutralize the spacecraft. Second, higher neutral densities result in shorter mean free paths for the beam electrons. Scattering of the beam electrons occurs closer to the spacecraft and fewer beam electrons escape. In the highest neutral density case of 10^{15} cm^{-3}, the potential is reduced to 10% of the beam energy. Also the spacecraft potential oscillations increase in frequency due to the large increase in the plasma density near the spacecraft.

Figure 8 shows phase space plots of beam and secondary electrons from a long simulation run, $\omega_{pe}t = 60$. The neutral density is 10^{14} cm^{-3}, the same as in Figures 4–6. At $\omega_{pe}t = 60$, many beam electrons have been scattered by collisions to lower velocities (Figure 8a). Particles at the beam front no longer travel at velocities comparable to the initial beam velocity. Note that newly injected beam electrons are travelling longer distances at nearly their initial injection velocity. They set up short wavelength beam-plasma oscillations which are apparent in the phase space plot. Figure 8b indicates that the secondary electrons are accelerated to velocities compararble to the beam velocity within the beam-plasma oscillation regions. These secondary electrons can be accelerated to the point where they contribute significantly to the collisional ionizations. A history of the spacecraft potential (Figure 9) shows that the potential is about 40% of the beam energy at $\omega_{pe}t = 30$ and is reduced to 25% of the beam energy at $\omega_{pe}t = 60$. Running the simulation for a longer time results in more secondary electrons produced near the spacecraft and also gives secondary electrons generated farther away from the spacecraft the time to respond to the positively charged spacecraft.

IV Radial Expansion of an Injected Electron Beam

A INTRODUCTION

Over the past 10 years, nonrelativistic electron beams have been injected into a background plasma and neutral gas to study beam propagation, instabilities, spacecraft charging, and other space plasma problems in the ionosphere [Grandal, 1982; Banks et al., 1987; Banks and Raitt, 1988; Kellogg et al., 1982; Sasaki et al., 1986]. Some experiments specifically examined the radial expansion characteristics of the beam [Banks et al., 1987; Banks and Raitt, 1988], indicating that the beam expansion characteristics depend in a complex way on beam propagation angle and spacecraft charging. Many simulation studies have studied the general relationship between spacecraft charging and the electron beam injection in the ionosphere [Omura and Matsumoto, 1984; Pritchett and Winglee, 1987; Okuda and Kan, 1987; Winglee and Pritchett, 1987; Okuda and Berchem, 1988; Winglee and Pritchett, 1988; Lin and Koga, 1989]. However, few have focused on understanding the radial expansion phenomenon. we therefore focus our simulation work on the beam radial expansion.

In the Vehicle Charging and Potential (VCAP) experiment on the Space Shuttle Orbiter mission, the STS-3 camera imaged a narrow collimation of an electron beam fired transverse to the magnetic field for 0.3 m before the light emission of the electron beam abruptly decreased [Banks et al., 1987; Banks and Raitt, 1988]. The reason for the sudden decrease in light emission is unclear. However, it may suggest that appreciable beam radial expansion seemed to occur due to an increase in the negative charge density of the beam. After the point of beam spreading, the beam evolved into a hollow cylindrical shell structure which propagated parallel to the local magnetic field. The vehicle electric potential induced by these electron beam firings was normally a few volts to a few tens of volts with a beam energy of 1 keV [Banks et al., 1987].

Space Experiments with Particle Accelerators (SEPAC) during the Spacelab 1 mission indicated that the electron beam injection had charged the spacecraft to a potential as high as the beam energy, which was 5 keV [Sasaki et al., 1986]. Because the ambient plasma cannot neutralize the electron beam and the spacecraft, the net beam charge and the spacecraft charging are important in this case in determining beam propagation and expansion.

In laboratory experiments, Kellogg et al. 1982] studied radial expansion of electron beams injected into a background plasma and neutral gas. When the electron gun was grounded, the envelope of the beam was twice the beam electron gyroridus radius ρ_e where $\rho_e = v_b/\Omega_{ce}$ for cross-field injection. For the aligned beam the radius of the envelope was $r_b \approx 0.25\rho_e$. However, when the electron gun was allowed to float and no background plasma was present,

the electron beam appeared to have a diameter approximately twice the beam electron gyroradius. In these cases the gun potential rose to the electron beam accelerator potential. Therefore, charging seems to play an important role in the beam radial expansion.

Several two-dimensional simulations show that high density electron beams can propagate in the plasma because the net beam charge has caused the beam to expand radially and reduced the beam density [Winglee and Pritchett, 1987; Okuda and Berchem, 1988; Winglee and Pritchett, 1988; Lin and Koga, 1989]. In particular, Winglee and Pritchett [1988] have simulated cross-field and parallel electron beam injection, concentrating on moderate spacecraft charging. For cross-field injection the beam is found to form a hollow cylinder of radius approximately equal to the beam gyroradius and width of about $2\lambda_{Db}$ where $\lambda_{Db} = v_b/\omega_b$. The beam width is believed to be caused by repulsive forces associated with a net negative charge within the beam. For parallel injection slower beam electrons are overtaken, causing a net repulsive force to push the beam electrons outward to a cylinder thickness comparable to the cross-field injection case. The maximum perpendicular velocity was found to be comparable to the parallel beam velocity.

Analytic calculations for electron beams injected parallel to magnetic field lines have shown that space charge effects play an important role during the initial phase of beam expansion [Gendrin, 1974]. Furthermore, the magnetic field determines the beam radius and beam density. However, the calculations did not take into account any possible beam instabilities.

In this project we study radial expansion of electron beams injected parallel to the magnetic field. We have used a two-dimensional electrostatic particle code to simulate the electron beam injection from an isolated finite equipotential conductor into a plasma. In contrast to Winglee and Prichett [1988], we concentrate on cases of high spacecraft charging, which are more applicable to SEPAC electron beam firings. It is shown that radial expansion is significant. We also surveyed the simulation results to determine the dependence of the beam expansion on the background magnetic field, beam density, and beam velocity.

To study radial expansion of an electron beam injected from a conductor, we used the same 2-D particle-in-cell code described in the previous section. In this study we neglected collisional ionization of neutrals by beam, background, and secondary electrons. We also neglected the high density neutral region at the right wall due to the relatively short timescale of these simulations. Again we present the simulation results in the electrostatic limit. Figure 10 illustrates the simulation geometry.

As in the previous simulations the ambient ions and electrons are initialized with Maxwellian velocity distributions and the same temperature, $T_e = T_i$ where T_e and T_i are the electron and ion temperatures, respectively.

B SIMULATION RESULTS

The simulation uses a $512\Delta \times 128\Delta$ grid in the x and y directions, respectively. The spacecraft is represented by a rectangular box centered at $x = 102\Delta$ and $y = 64\Delta$ with size $4\Delta \times 32\Delta$ in the x and y directions, respectively. The grid size, Δ, equals the Debye length of the ambient electrons defined as $\lambda_d = a_c/\omega_{pe}$ where $a_c = (2T_e/m_e)^{1/2}$ is the thermal velocity of the ambient electrons and ω_{pe} is the ambient electron plasma frequency. We choose the ion to electron mass ratio to be 100, and $a_c = 0.001c$ where c is the speed of light, a unit of the simulation. We use a reference electron gyrofrequency Ω_{ce} of $0.25\omega_{pe}$, which is close to the ionospheric value of $0.3\omega_{pe}$. The simulations use a time step $\Delta t = 0.05\omega_{pe}^{-1}$ and 131,072 particles for the ambient plasma. For the reference case the electron beam has a width of 4Δ, an injection velocity of $v_b = 10a_c$ along the x axis, zero initial thermal velocity, and a density ratio of $n_b/n_c = 10$.

Figures 11-13 show results of electron beam injection for the reference parameters. The phase space plot $x - v_x$ at $\omega_{pe}t = 30$ in Figure 11a indicates that the point at which beam electrons are stopped (stagnation point) is very close to the conductor surface. Due to the high beam density the spacecraft becomes positively charged, causing the beam electrons to be rapidly drawn back to the spacecraft surface. The average electrostatic potential of the spacecraft in this case is $\approx 94\%$ of the beam energy. Some electrons at the front of the beam are accelerated to velocities higher than the original beam velocity. This is due to the bunching of beam electrons behind the beam head. Also some returning beam electrons overshoot the spacecraft and are drawn back on the wake side. The configuration space plot given in Figure 11b shows that the electron beam expands radially. Figure 12a shows a contour plot of the beam density where the contour line delineates the beam edge. From this plot the beam radius is approximately $r_b = 40\Delta$. The beam electron gyroradius $\rho_e = v_b/\Omega_{ce}$ is also 40Δ where v_b is the initial beam velocity. It is apparent from earlier configuration space plots that the maximum beam expansion occurs near the stagnation point, which is very close to the spacecraft surface. The highest beam density is at the stagnation point of the beam (Figure 12b). This is in agreement with analytical results for one-dimensional electron beam injection into a vacuum [Parks et al., 1975]. Physically, the high density at the stagnation point is understood in an approximate sense by the conservation of flux $n_b v_b$. At the stagnation point, where the average beam velocity is smallest, the density should be highest assuming substantial expansion of the beam has not occurred.

Figures 13a and 13b show that the maximum transverse electric field E_y and the maximum longitudinal electric field E_x occur where the beam density is highest. The transverse velocities to which the beam electrons are accelerated depend on the time spent in the stagnation region, where the transverse electric fields are largest. This can be estimated from the width of the trans-

verse electric field region, approximately 8Δ, and the initial beam velocity. From these values it is apparent that the beam particles can be accelerated to 75% of the initial beam velocity. In general beam electrons travel through the stagnation region with velocities lower than the initial beam velocity so that they spend more time in the stagnation region and are accelerated to higher velocities. After the stagnation region, the transverse electric field E_y is smaller (Figure 13a) and the average beam velocity is higher (Figure 11a). Therefore, the beam electrons receive their largest tranverse kick very close to the spacecraft and experience smaller transverse impulses from that point on.

C Variation with Magnetic Field Strength

Figure 14 shows beam density plots at $\omega_{pe}t = 30$ where the contour lines indicate the beam envelope. The magnetic field Ω_{ce}/ω_{pe} is 0.25, 0.5, and 1.0 down the page with all other parameters fixed. Note that the maximum beam radius decreases with increasing magnetic field. The ratio of the maximum beam radius to the electron gyroradius r_b/ρ_e is approximately 1 for each of these cases. This indicates that the beam electrons receive the same transverse kick independent of the magnetic field and expand to ρ_e in the range of ionospheric magnetic field values. In Figure 14c, where $\Omega_{ce}/\omega_{pe} = 1.0$, no beam electrons are in the wake region of the spacecraft. The maximum width beam electrons achieve, $2\rho_e$, is smaller than the spacecraft width. Therefore all returning beam electrons strike the spacecraft surface.

D Variation with Beam Density

Figure 15 shows simulation results at $\omega_{pe}t = 30$ varying the beam to ambient plasma density ratio n_b/n_c from 1 to 20 for the cases of $\Omega_{ce}/\omega_{pe} = 0.25$ (solid line) and 0.5 (dotted line). The ratio r_b/ρ_e is between 0.725 for $n_b/n_c = 1$ and 1.3 for $n_b/n_c = 20$. The maximum beam radius gradually increases with beam density. This indicates that the transverse kick that the beam electrons receive gradually increases with beam density. The relative magnitude of the transverse kick can be obtained from the average velocity of the beam electrons through the stagnation region. The average velocity gives a rough idea of the time that the beam electrons are accelerated by the transverse electric field E_y in the stagnation region. Figure 16 shows the average velocity of beam electrons at the stagnation point versus beam density for $\Omega_{ce}/\omega_{pe} = 0.25$ (solid line) and 0.5 (dotted line) at $\omega_{pe}t = 30$. The velocity is averaged across the beam and the stagnation point is taken to be the point where the longitudinal electric field E_x is a maximum. The average velocity decreases with increasing beam density for both values of the magnetic field. This indicates that beam electrons spend more time in the stagnation region for higher density beams and are, therefore, accelerated to higher transverse velocities. The ratio of the electron beam Debye length λ_{Db} to the ambient electron Debye length λ_d,

which is

$$\frac{\lambda_{Db}}{\lambda_d} = (\frac{v_b}{a_c})(\frac{n_c}{n_b})^{1/2}, \tag{4}$$

gives an understanding of this velocity trend. The electron beam Debye length is an indication of the charge separation distance between the spacecraft and the beam stagnation point. The ambient electron Debye length indicates the distance above which ambient electrons neutralize excess charge. As this ratio decreases the beam electrons feel the Coulombic potential of the spacecraft more since ambient electrons have a harder time shielding the effects of the retarding potential drop. Therefore, the beam electrons travel with lower velocities. This ratio decreases with increasing beam density n_b as $n_b^{-1/2}$ following the trend of the average velocity in Figure 16.

E Variation with Beam Velocity

Figure 17 shows the beam radius normalized to the electron gyroradius r_b/ρ_e as a function of initial injection velocity v_b at $\omega_{pe}t = 30$. The injection velocity v_b/a_c where a_c is the ambient electron thermal velocity is varied between 2.5 and 20.0. All other parameters are the same as in the reference case. The radial expansion is largest for low velocity injection and smallest for high velocity injection. The relative magnitude of the transverse kick can again be inferred from the average velocity of the beam electrons through the stagnation region. Figure 18 shows the average velocity of beam electrons at the stagnation point versus initial beam injection velocity of $\omega_{pe}t = 30$. The average velocity increases with the initial beam injection velocity. Beam electrons spend more time in the stagnation region for lower injection velocities and are, therefore, accelerated to higher relative transverse velocities. This velocity trend can also be interpreted from the ratio of the beam electron Debye length to the ambient electron Debye length. This ratio increases linearly with the initial beam injection velocity. As the beam injection velocity increases, the ambient electrons are more able to shield excess charge buildup over the beam electron Debye length. Therefore, the beam electrons travel with higher velocities through the stagnation region, which is in agreement with Figure 18.

V DISCUSSION

We have simulated the injection of a nonrelativistic electron beam from a finite conductor with a beam density much larger than the ambient density, $n_b/n_o = 10$, and have incorporated secondary electron and ion production due to collisional ionizations. The simulation results suggest that the uniform neutral background reduces the amount of spacecraft charging. Collisional ionization of the neutral particles by beam electrons results in an increase of secondary electrons. These secondary electrons help neutralize the spacecraft. The positively charged spacecraft accelerates background electrons to velocities high enough for them to ionize neutral particles, producing secondary electrons and ions in the wake region of the spacecraft. Another interesting result is that the stagnation point of the electron beam moves farther away from the spacecraft. As the spacecraft potential decreases, the beam electrons are able to travel longer distances before being stopped.

In this report we have examined the initial responses of electrons after an electron beam injection. The simulation runs for longer time periods indicate that charging is further reduced at later times, allowing newly injected beam electrons to leave the spacecraft region with a small decrease in their velocities. These electrons set up short wavelength beam-plasma oscillations which accelerate secondary electrons to velocities close to the beam velocity.

We have examined the radial expansion properties of a nonrelativistic electron beam injected along magnetic field lines into a background plasma. We have concentrated on high beam current cases where spacecraft charging is significant. In our reference case with $n_b/n_c = 10$ and $v_b/a_c = 10$, the beam expandes to twice the beam electron gyroradius ρ_e. The beam electrons receive a large transverse kick from beam electrons which have built up at the stagnation point. This kick, which occurs very close to the injection point, determines the beam envelope from that point on. We have found that the transverse energization of the beam electrons is independent of the strength of the magnetic field for values between $\Omega_{ce}/\omega_{pe} = 0.25$ and 1. The beam envelope is twice the beam electron gyroradius ρ_e. We have also found that the beam envelope increases with beam density. The average velocity of beam electrons through the stagnation region decreases with increasing beam density. The average velocity determines the time spended by beam electrons in the stagnation region and, therefore, the duration in which beam electrons are accelerated by the transverse electric fields. The final transverse velocity of the beam electrons, and thus the beam envelope increases with beam density. Variation of the initial beam injection velocity indicates that the beam envelope decreases with increasing beam injection velocity. The average velocity of beam electrons through the stagnation region increases with beam injection velocity. Therefore, beam electrons with high injection velocity are accelerated to lower relative transverse velocities than beam electrons with low injection velocities. The ratio of λ_{Db}/λ_d, which is an indication of how well beam elec-

trons are shielded from the charged spacecraft surface by the ambient electrons, can be used to explain the dependence of beam radius on beam density and beam injection velocity. This dependence is evident from Figure 16 where the average beam velocity at the stagnation point drops off approximately as $n_b^{-1/2}$ and from Figure 18 where the average velocity increases almost linearly with beam injection velocity v_b.

The spacecraft potential energy in each of these runs varied between 60% and 100% of the beam energy except for the cases of low beam density. These results are most applicable to the SEPAC electron beam injection experiments where the Shuttle was charged to the beam energy.

REFERENCES

Banks, P. M. and G. Kockarts,"Aeronomy", Academic Press, New York, 1973.

Banks, P. M., W. J. Raitt, A. B. White, R. I. Bush, and P. R. Williamson, "Results from the vehicle charging and potential experiment on STS-3", *J. Spacecr. Rockets*, vol. 24, p. 138, 1987.

Banks, P. M. and W. J. Raitt, "Observations of electron beam structure in space experiments", *J. Geophys. Res.*, vol. 93, p. 5811, 1988.

Gendrin, R., "Initial expansion phase of artificially injected electron beam", *Planet. Space Sci.*, vol. 22, p. 633, 1974.

Grandal, B., ed., " Artificial Particle Beams in Space Plasma Studies", Plenum, New York, 1982.

Gurnett, D. A., W. S. Kurth, J. T. Steinberg, P. M. Banks, R. I. Bush, and W. J. Raitt, "Whistler-mode radiation from the Spacelab-2 electron beam", *Geophys. Res. Lett.*, vol. 13, no. 3, p. 225, 1986.

Hockney, R. W. and J. W. Eastwood, "Computer simulation using particles", McGraw-Hill, New York, 1981.

Katz, I., A. Jongeward, D. E. Parks, D. L. Reasoner, and C. K. Purvis, "Energy broadening due to space-charge oscillations in high current electron beams", *Geophys. Res. Lett.*, vol. 13, no. 1, p. 64, 1986.

Kellogg, P. J., H. R. Anderson, W. Bernstein, T. J. Hallinan, H. R. Holzworth, R. J. Jost, H. Leinbach, and E. P. Szuszuczewicz, "Laboratory simulation of injection particle beams in the ionosphere", *Artificial Particle Beams in Space Plasma Studies*, edited by Bjorn Grandel, 1982, pp. 289-329.

Lin, C. S. and J. K. Koga, "Spacecraft charging potential during electron-beam injections into space plasmas", *IEEE Trans. Plasma Sci.*, vol. 17, no. 2, p. 205, 1989.

Machida, S. and C. K. Goertz, "The electromagnetic effect on the critical ionization velocity process", *J. Geophys. Res.*, vol. 93, no. A10, p. 11495, 1988.

Marshall, J. A., C. S. Lin, J. L. Burch, T. Obayashi, C. Beghin, "Spacelab 1 experiments on interactions of an energetic electron beam with neutral gas", *J. Spacecr Rockets*, vol. 25, no. 5, p. 361, 1988.

Nelson, C. W. and H. R. Lewis, "Particle simulation techniques in the nonradiative limit", *Methods Comput. Phys.* vol. 16, p. 367, 1976.

Okuda, H., and J. R. Kan, "Injection of an electron beam into a plasma and spacecraft charging", *Phys. Fluids*, vol. 30, No. 1, p. 209, 1987.

Okuda, H., and J. Berchem, "Injection and Propagation of a nonrelativistic electron beam and spacecraft charging", *J. Geophys. Res.*, vol. 93, no. A1, p. 175, 1988.

Omura, Y. and H. Matsumoto, "Computer simulations of beam injection experiments for SEPAC/Spacelab 1 mission", *Radio Sci.*, vol. 19, no. 2, p. 496, 1984.

Papdopoulos, K. and E. P. Szuszczewicz, "Current Understanding and issues on electron beam injection in space", *Adv. Sapce Res.*, vol. 8, no. 1, p. 101, 1989.

Parks, D. E., A. R. Wilson, and I. Katz, "Monode plasma sheath dynamics", *IEEE trans. Nucl. Sci.*, vol. NS-22, no. 6, p. 2368, 1975.

Pritchett, P. L. and R. M. Winglee, "The plasma environment during particle beam injection into space plasmas, 1, electron beams", *J. Geophys. Res.*, vol. 92, no. A7, p. 7673, 1987.

Sasaki, S., N. Kawashima, K. Kuriki, M. Yanagisawa, and T. Obayashi, "Vehicle charging observed in SEPAC Spacelab-1 experiment", *J. Spacecr Rockets*, vol. 23, no. 2, p. 129, 1986.

Sasaki, S., N. Kawashima, K. Kuriki, M. Yanagisawa, T. Obayashi, W. T. Roberts, D. L. Reasoner, P. R. Williamson, P. M. Banks, W. W. L. Taylor, K. Akai, and J. L. Burch, "Neutralization of beam-emitting spacecraft by plasma injection", *J. Spacecr Rockets*, vol. 24, no. 3, p. 227,1987.

Szuszczewicz, E. P., *J. Atm. Terr. Phys.*, vol. 47, p 1189, 1985.

Winglee, R. M., and P. L. Pritchett, "Space charge effects during the injection of dense electron beams into space plasmas", *J. Geophys. Res.*, vol. 92, no. A6, p. 6114, 1987.

Winglee, R. M., and P. L. Pritchett, "Comparative study of cross-field and field-aligned electrons beams in active experiments", *J. Geophys. Res.*, vol. 93, no. A6, p. 5823, 1988.

Winglee, R. M., "Spacecraft charging during electron beam injection and turnoff", in Spacecraft Charging Technology Conference proceedings, Monterey, California, 1989.

FIGURE CAPTIONS

Figure 1. Simulation configuration.

Figure 2. Results of simulation for $n_b/n_o = 10$ and $v_b/a_c = 10$ at $\omega_{pe}t = 30$. (a) The beam electron phase space in the x - v_x plane and (b) the positions of beam electrons in the x - y plane. The position is normalized by the Debye length and the velocity is normalized the beam velocity.

Figure 3. Time history of the conductor potential, ϕ_o, normalized to the beam energy E_b. For this simulation, $n_b/n_o = 10$ and $v_b/a_c = 10$.

Figure 4. Results of simulation with a uniform neutral background for $n_b/n_o = 10$ and $v_b/a_c = 10$ at $\omega_{pe}t = 30$. (a) The beam electron phase space in the x - v_x plane and (b) the positions of beam electrons in the x - y plane.

Figure 5. Results of simulation with a uniform neutral background (a) The secondary electron phase space in the x - v_x plane and (b) the positions of secondary electrons in the x - y plane.

Figure 6. Time history of the conductor potential, ϕ_o, normalized to the beam energy E_b.

Figure 7. Spacecraft potential versus neutral density.

Figure 8. Results of simulation with a uniform neutral background at $\omega_{pe}t = 60$. (a) The beam electron phase space in the x - v_x plane and (b) the secondary electrons in the x - v_x plane.

Figure 9. Time history of the conductor potential, ϕ_o, for $\omega_{pe}t = 60$.

Figure 10. Simulation configuration.

Figure 11. Results of simulation for $n_b/n_c = 10$ and $v_b/a_c = 10$ at $\omega_{pe}t = 30$. (a) The beam electron phase space in the x-v_x plane and (b) the positions of beam electrons in the x-y plane. The position is normalized by the Debye length and the velocity is normalized by the initial beam injection velocity.

Figure 12. Density plots of beam electrons at $\omega_{pe}t = 30$ for $n_b/n_c = 10$ and $v_b/a_c = 10$. (a) Contour lines delineate beam envelope. (b) Profile of beam density along beam showing maximum density close to spacecraft surface.

Figure 13. Profiles of maximum field quantities across beam at $\omega_{pe}t = 30$. (a) Maximum transverse electric field E_y and (b) maximum longitudinal

electric field E_x.

Figure 14. Density plots of beam electrons at $\omega_{pe}t = 30$ for $n_b/n_c = 10$ and $v_b/a_c = 10$. Contour lines delineate beam envelope. Ω_{ce}/ω_{pe} = (a) 0.25, (b) 0.5, and (c) 1.0

Figure 15. Electron beam envelope radius r_b/ρ_e versus n_b/n_c at $\omega_{pe} = 30$ for $v_b/a_c = 10$.

Figure 16. Average velocity v_x at the stagnation point normalized to ambient electron thermal velocity a_c versus n_b/n_c at $\omega_{pe} = 30$ for $v_b/a_c = 10$.

Figure 17. Electron beam envelope radius r_b/ρ_e versus initial beam injection velocity v_b/a_c at $\omega_{pe} = 30$ for $n_b/n_c = 10$.

Figure 18. Absolute value of average velcity v_x at the stagnation point normalized to ambient electron thermal velocity a_c versus initial injection velocity v_b/a_c at $\omega_{pe} = 30$ for $n_b/n_c = 10$.

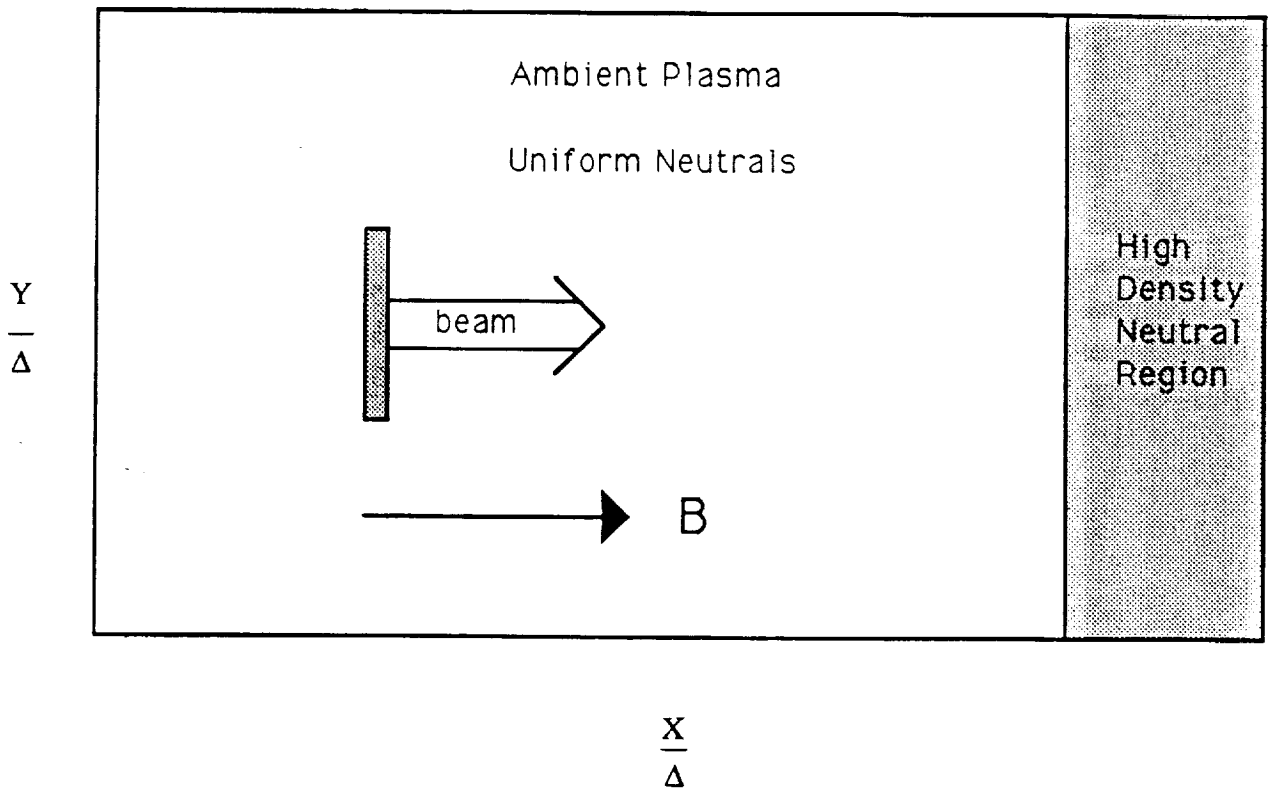
Ambient Plasma
Uniform Neutrals
beam
B
High Density Neutral Region
Y/Δ
X/Δ

Figure 1

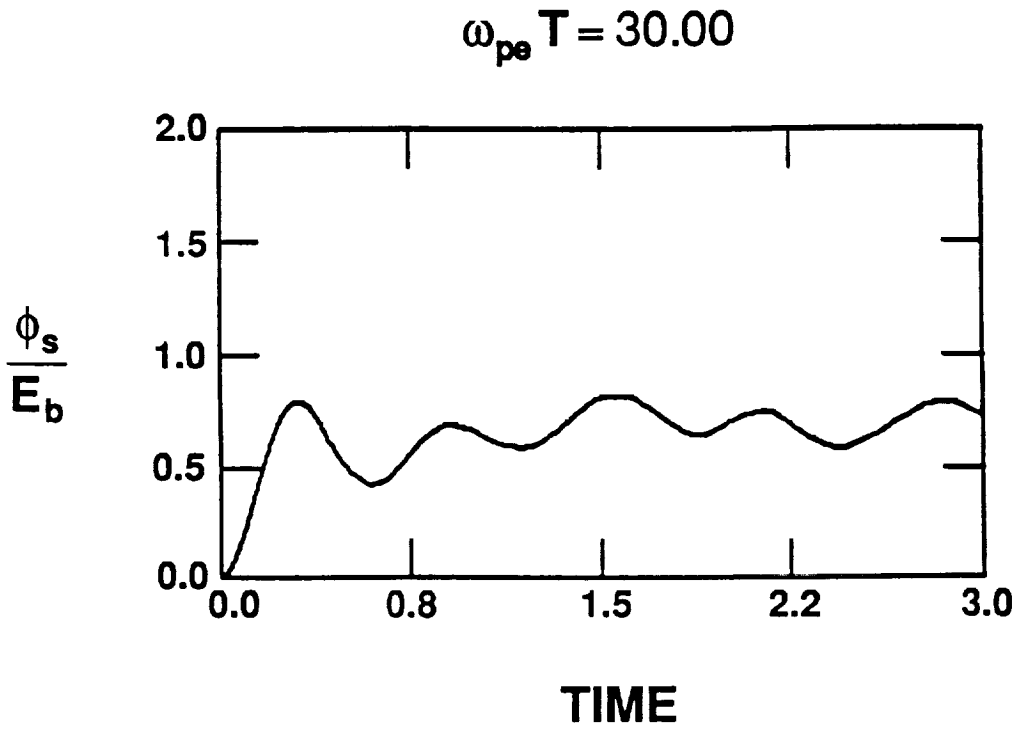

Figure 2

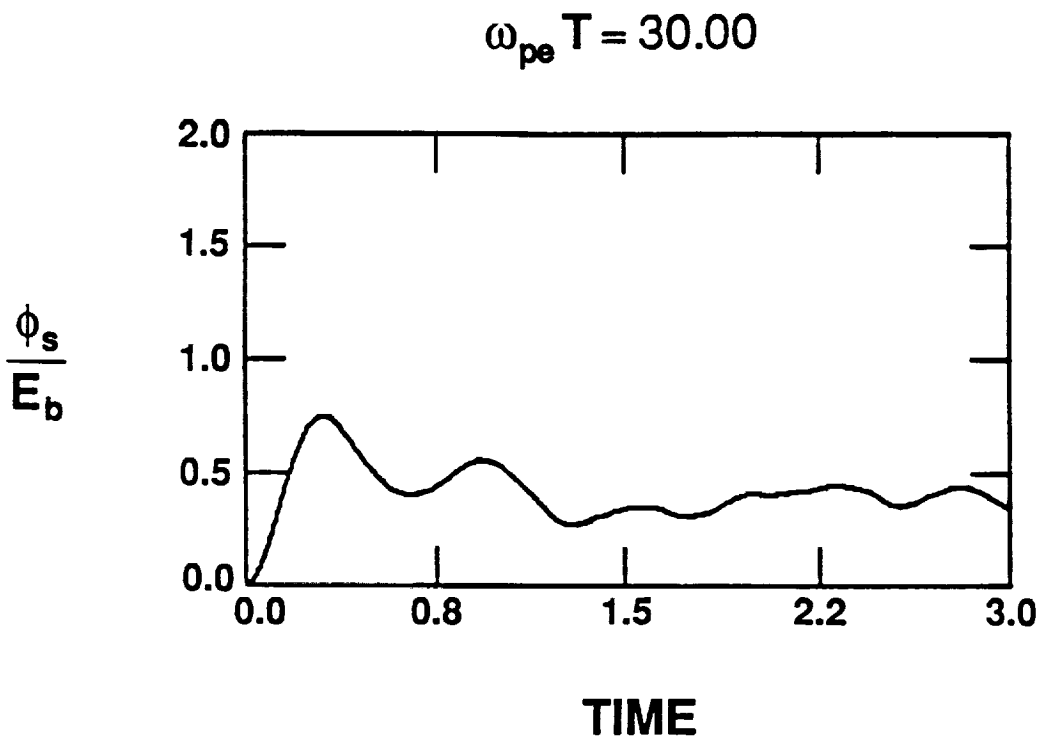

Figure 3

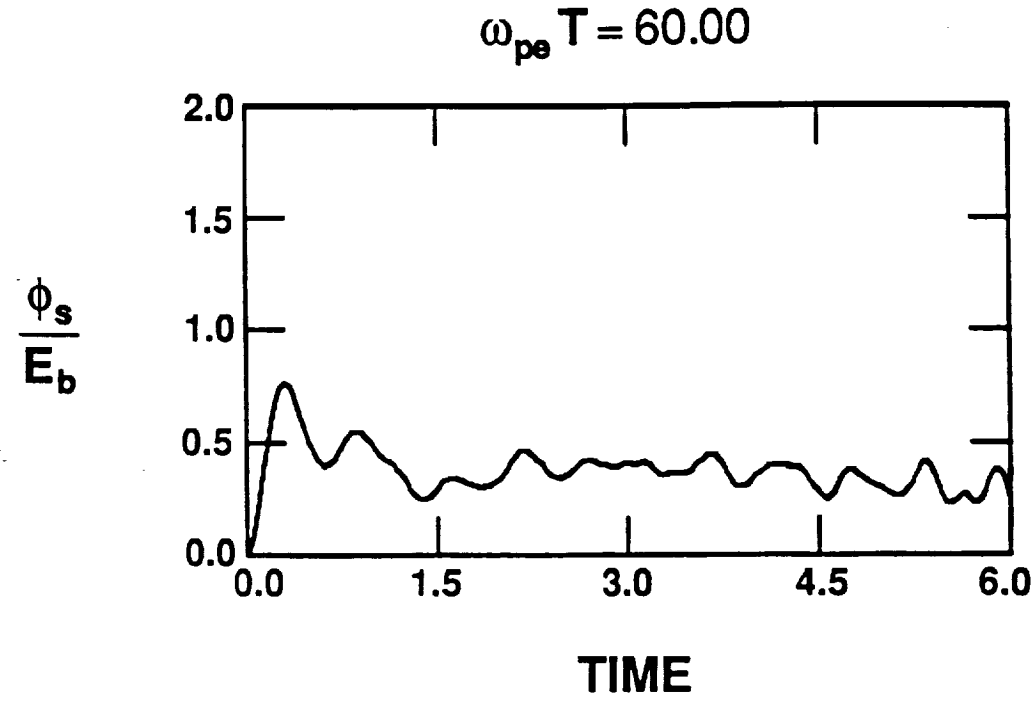

Figure 4

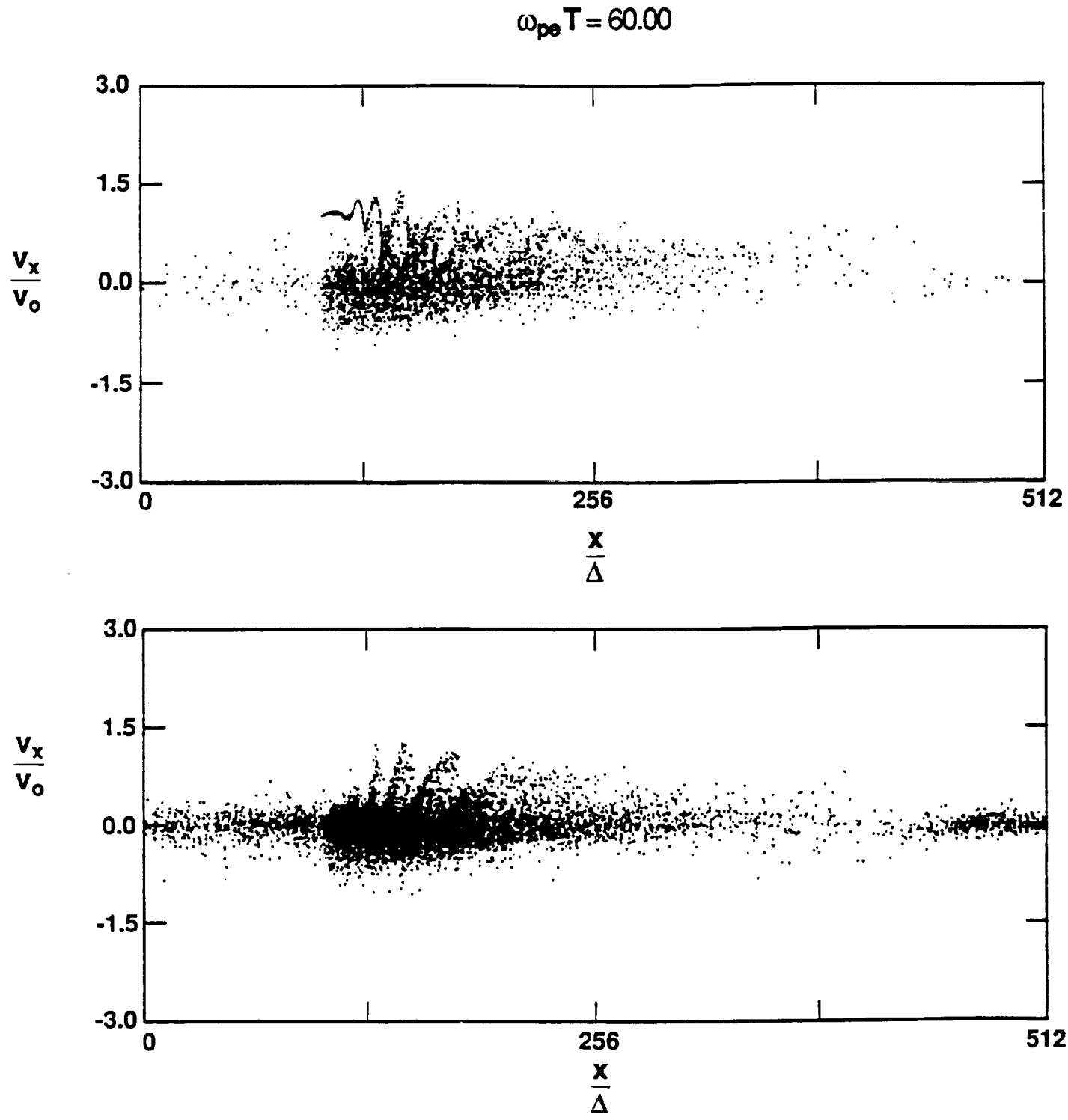
$\omega_{pe}T = 60.00$
3.0
1.5
0.0
-1.5
-3.0
$\frac{v_x}{v_o}$
0
256
512
$\frac{x}{\Delta}$
3.0
1.5
0.0
-1.5
-3.0
$\frac{v_x}{v_o}$
0
256
512
$\frac{x}{\Delta}$

Figure 5

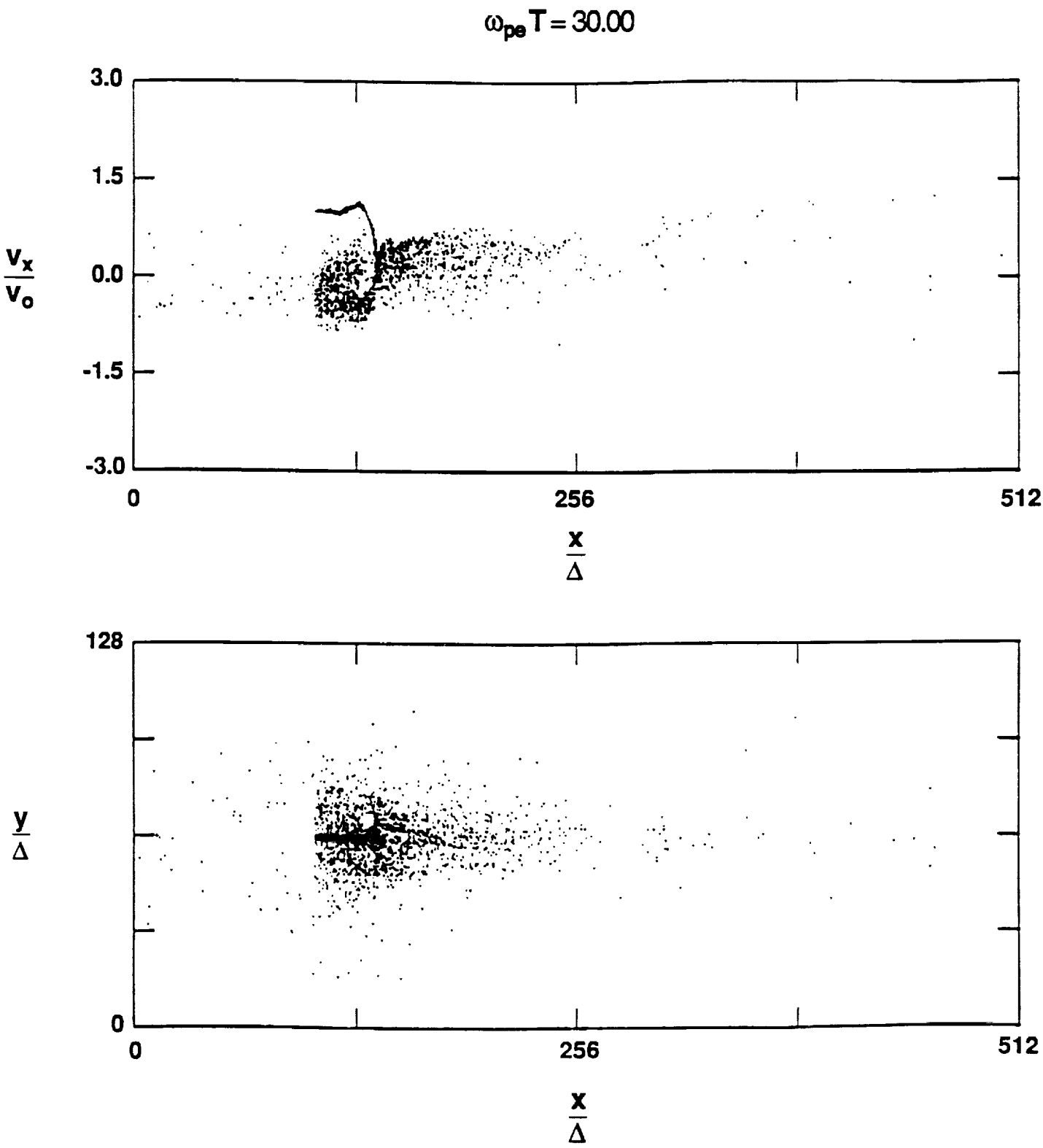
$\omega_{pe}T = 30.00$
3.0
1.5
0.0
-1.5
-3.0
$\frac{v_x}{v_o}$
0
256
512
$\frac{x}{\Delta}$
128
0
$\frac{y}{\Delta}$
0
256
512
$\frac{x}{\Delta}$

Figure 6

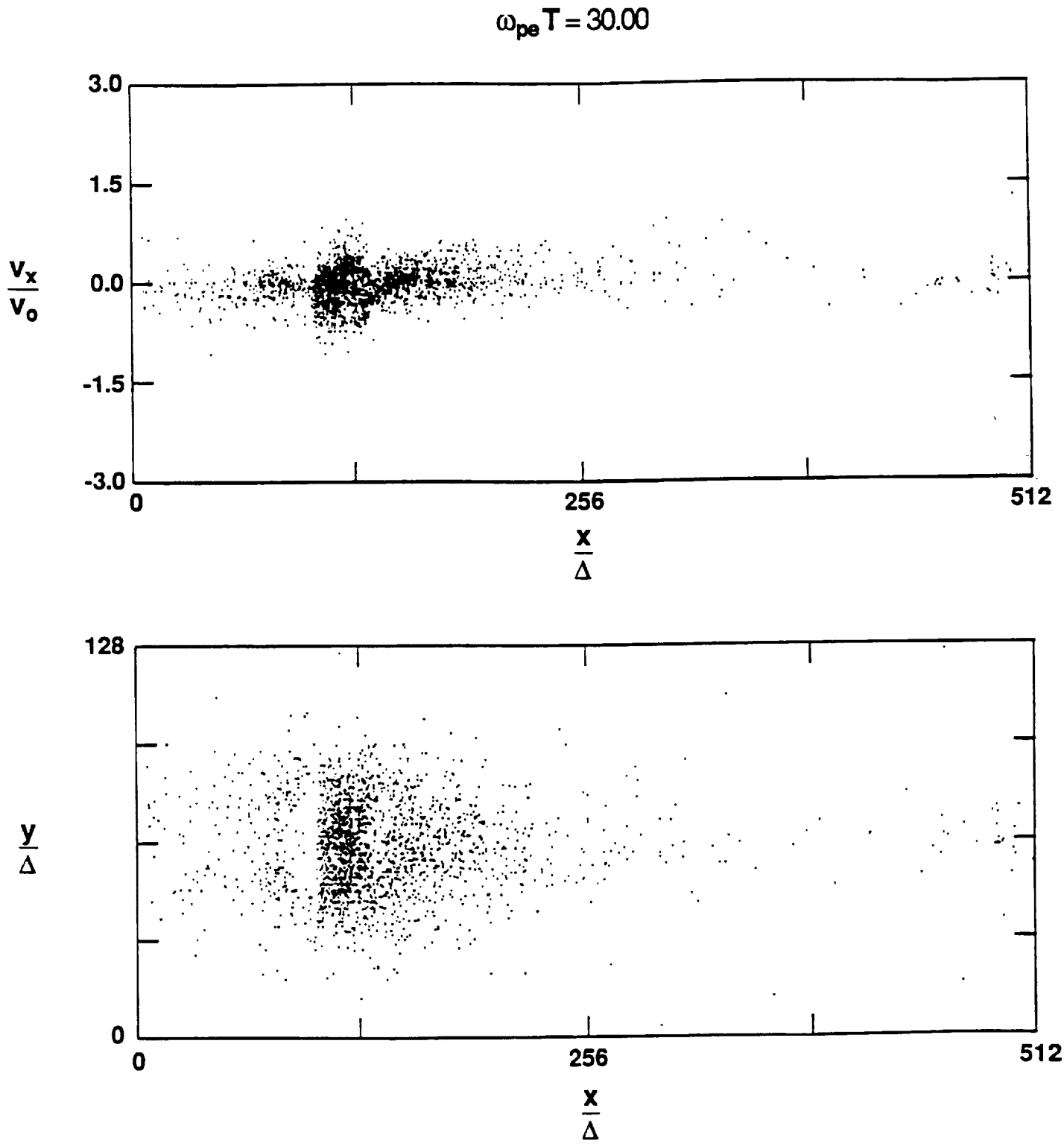
$\omega_{pe} T = 30.00$
3.0
1.5
0.0
-1.5
-3.0
$\frac{v_x}{v_o}$
0
256
512
$\frac{x}{\Delta}$
128
0
$\frac{y}{\Delta}$
0
256
512
$\frac{x}{\Delta}$

Figure 7

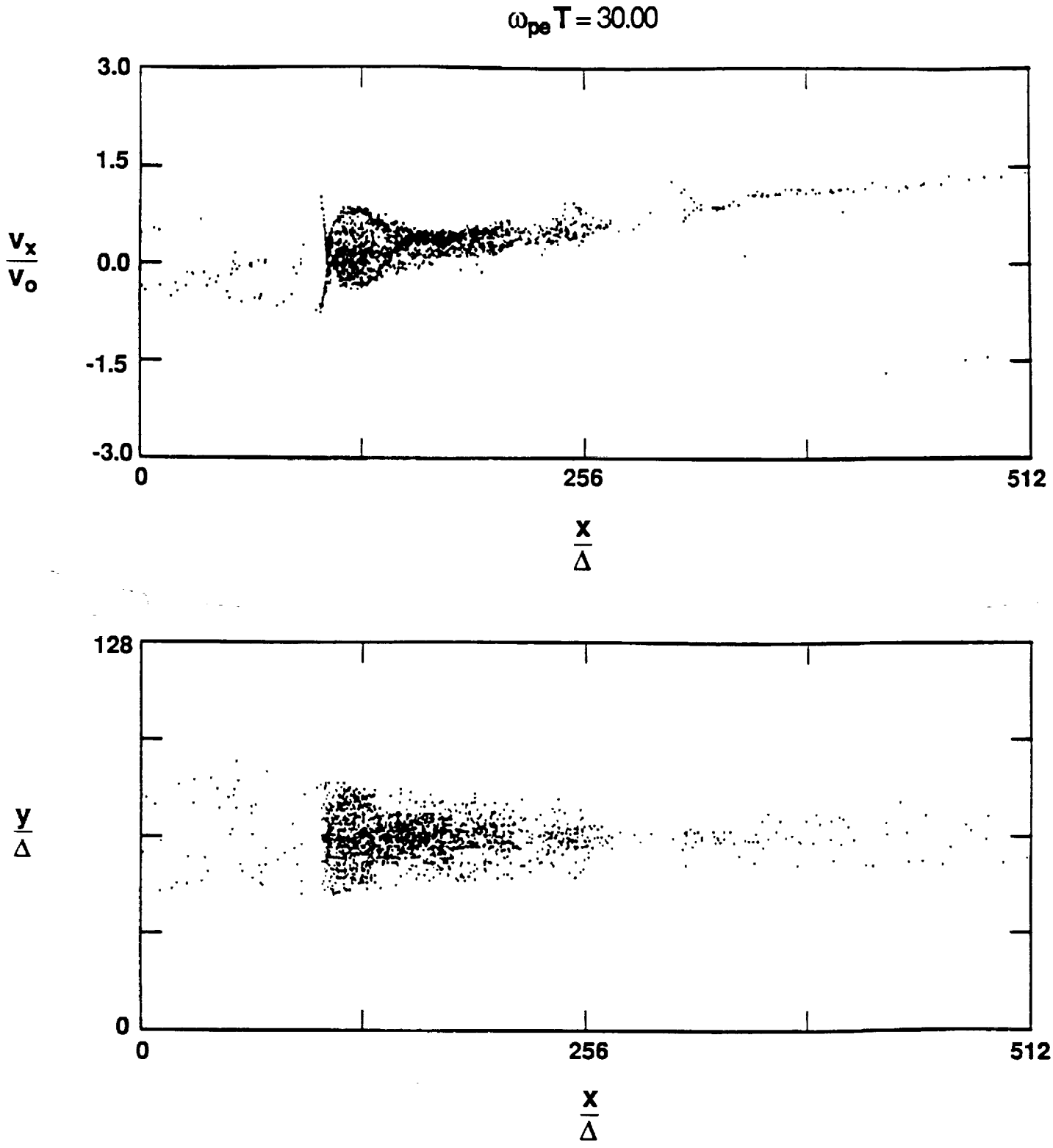
$\omega_{pe}T = 30.00$
3.0
1.5
0.0
-1.5
-3.0
$\frac{v_x}{v_o}$
0
256
512
$\frac{x}{\Delta}$
128
0
$\frac{y}{\Delta}$
0
256
512
$\frac{x}{\Delta}$

Figure 8

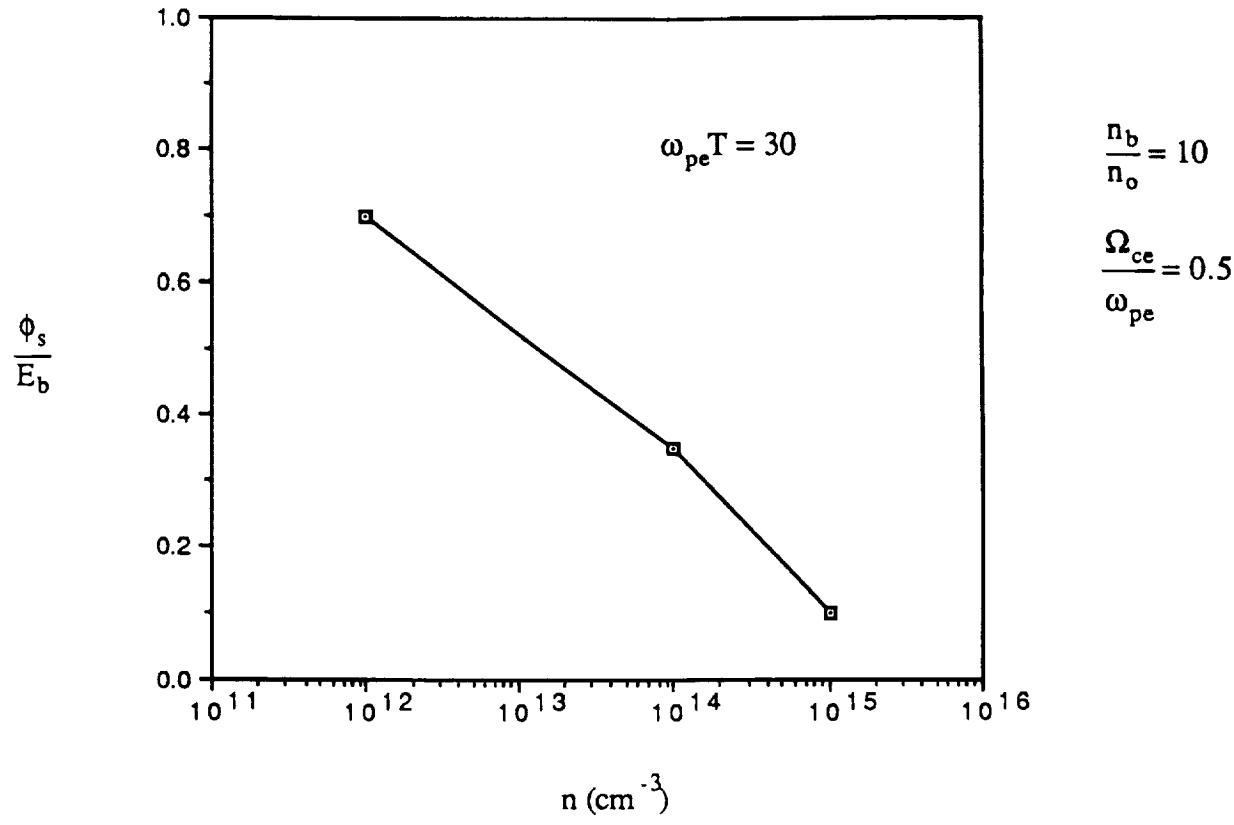
1.0
0.8
0.6
0.4
0.2
0.0
$\omega_{pe}T = 30$
$\frac{n_b}{n_o} = 10$
$\frac{\Omega_{ce}}{\omega_{pe}} = 0.5$
$\frac{\phi_s}{E_b}$
10^{11}
10^{12}
10^{13}
10^{14}
10^{15}
10^{16}
n (cm^{-3})

Figure 9

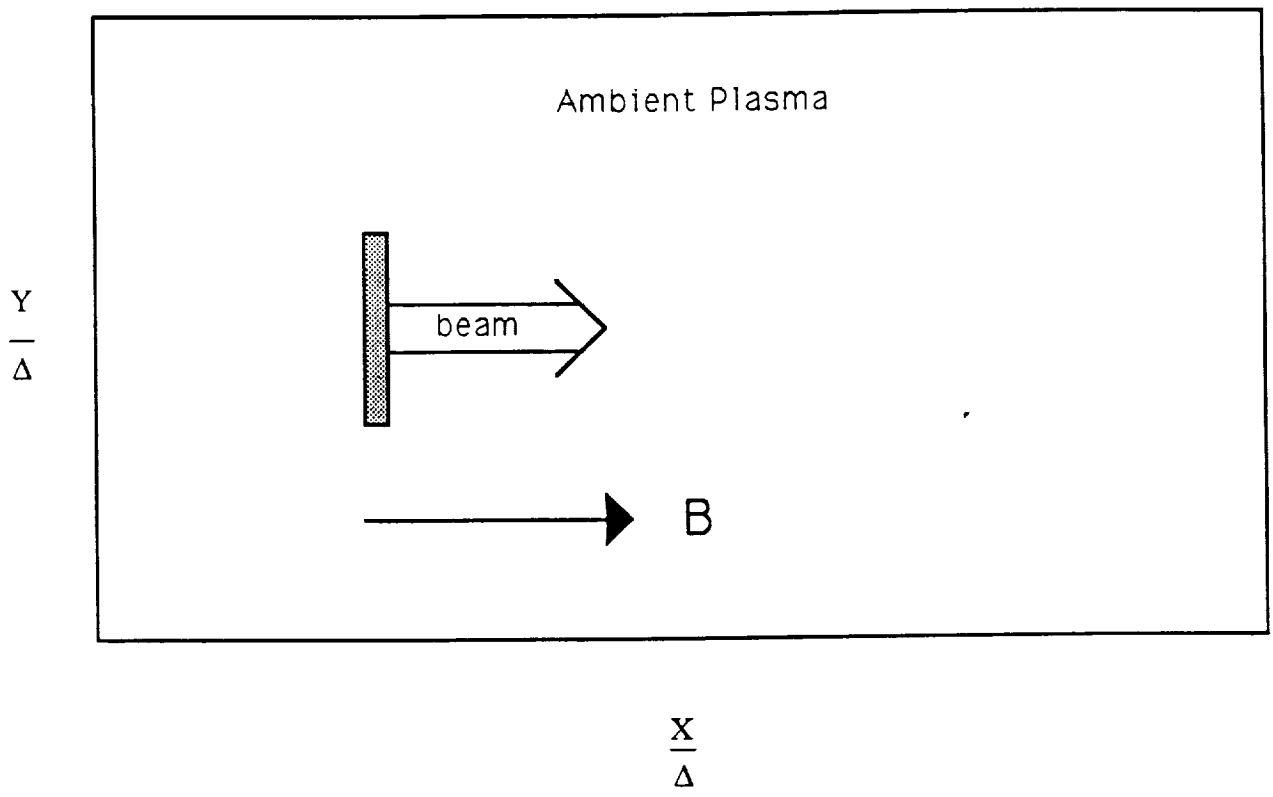

Figure 10

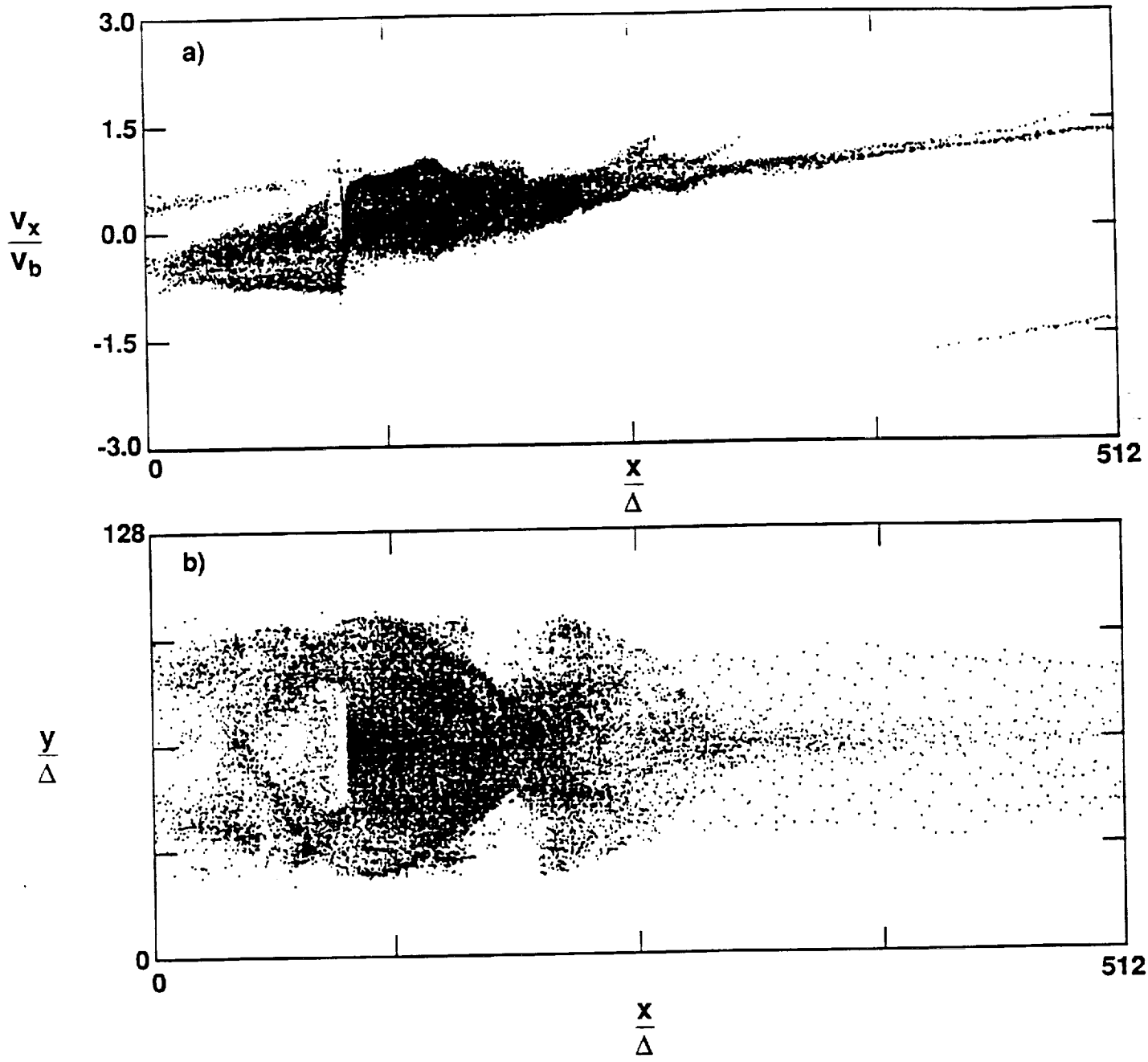
3.0
a)
1.5
$\frac{v_x}{v_b}$
0.0
-1.5
-3.0
0
512
$\frac{x}{\Delta}$
128
b)
$\frac{y}{\Delta}$
0
0
512
$\frac{x}{\Delta}$

Figure 11

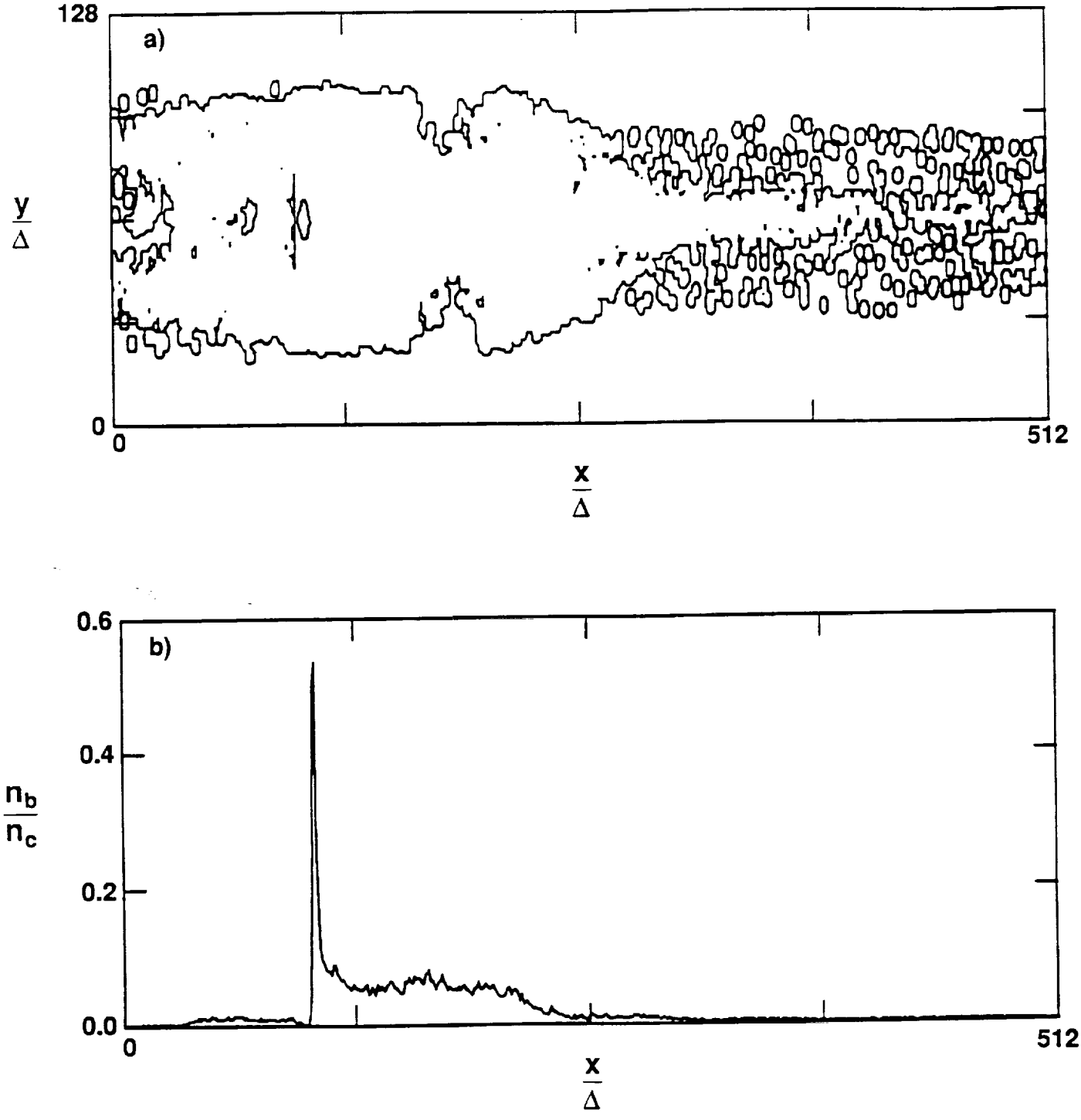

Figure 12

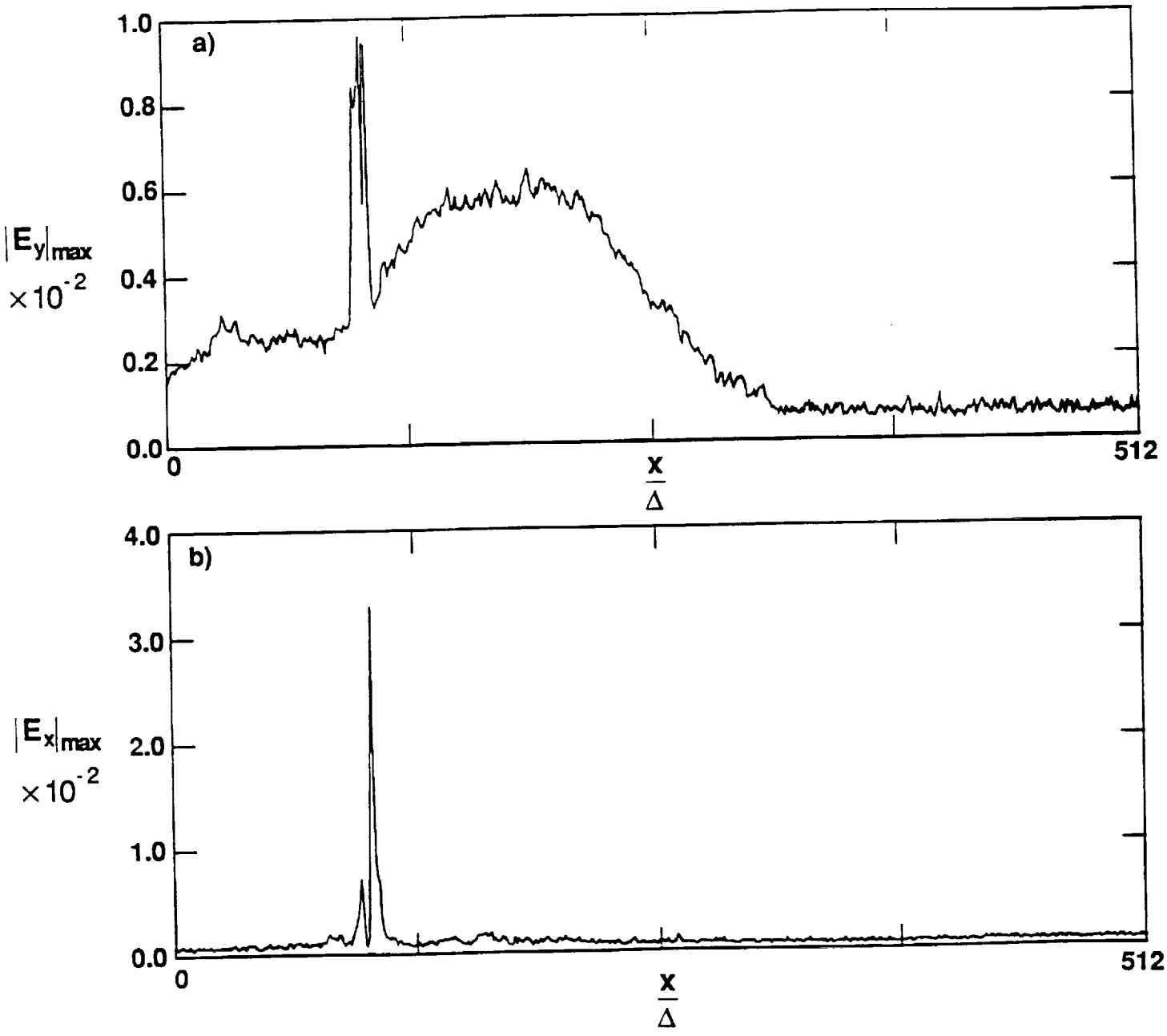
a)
1.0
0.8
0.6
0.4
0.2
0.0
$|E_y|_{max}$
$\times 10^{-2}$
0
512
$\frac{x}{\Delta}$
b)
4.0
3.0
2.0
1.0
0.0
$|E_x|_{max}$
$\times 10^{-2}$
0
512
$\frac{x}{\Delta}$

Figure 13

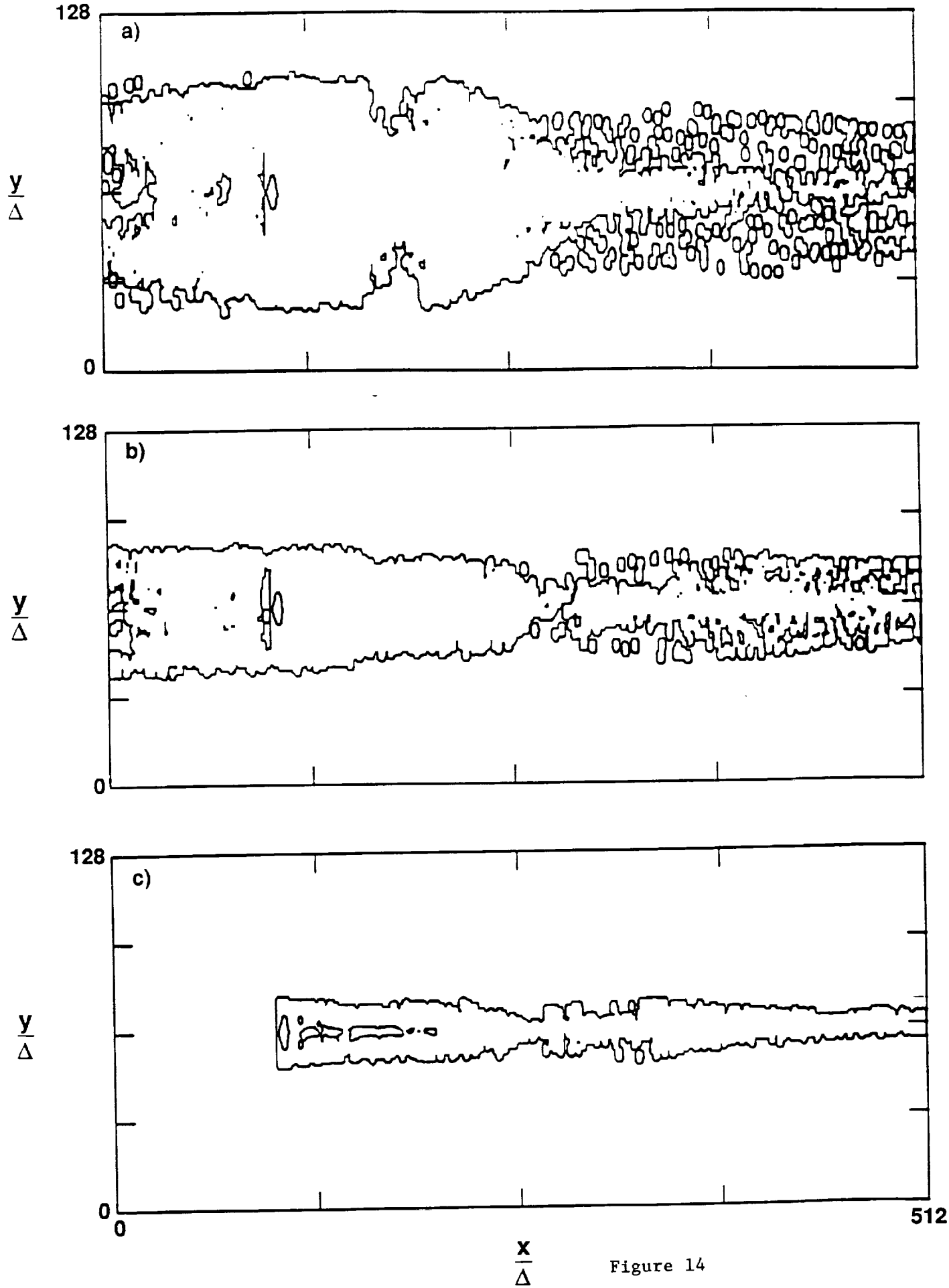

Figure 14

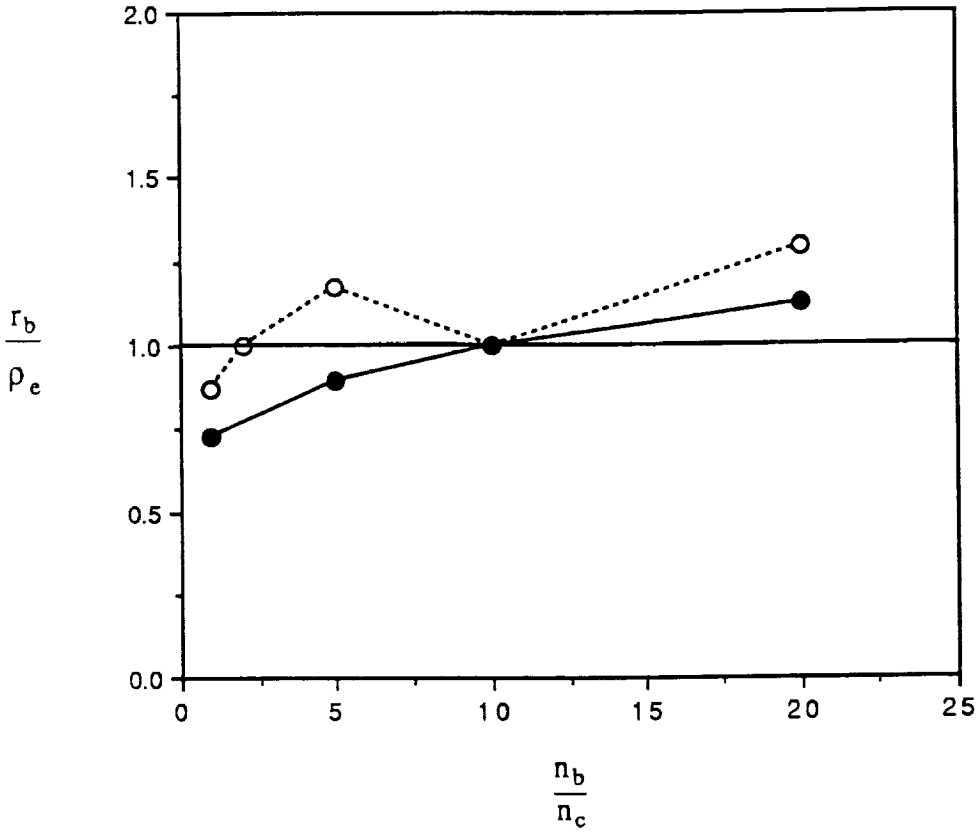

Figure 15

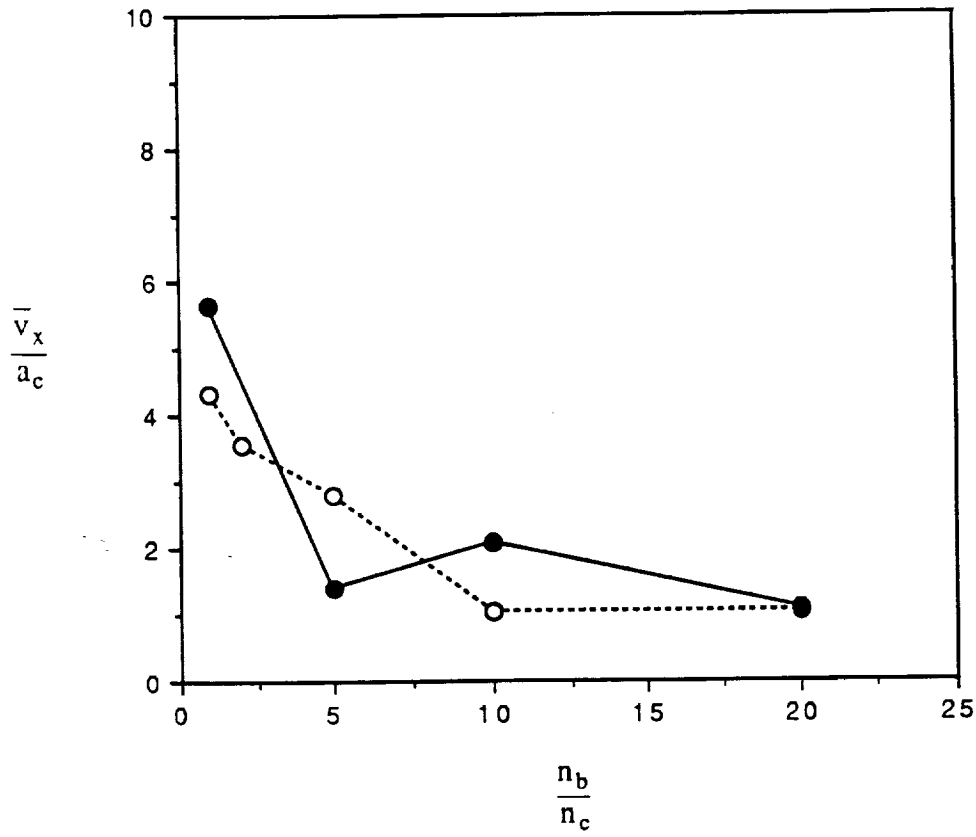

Figure 16

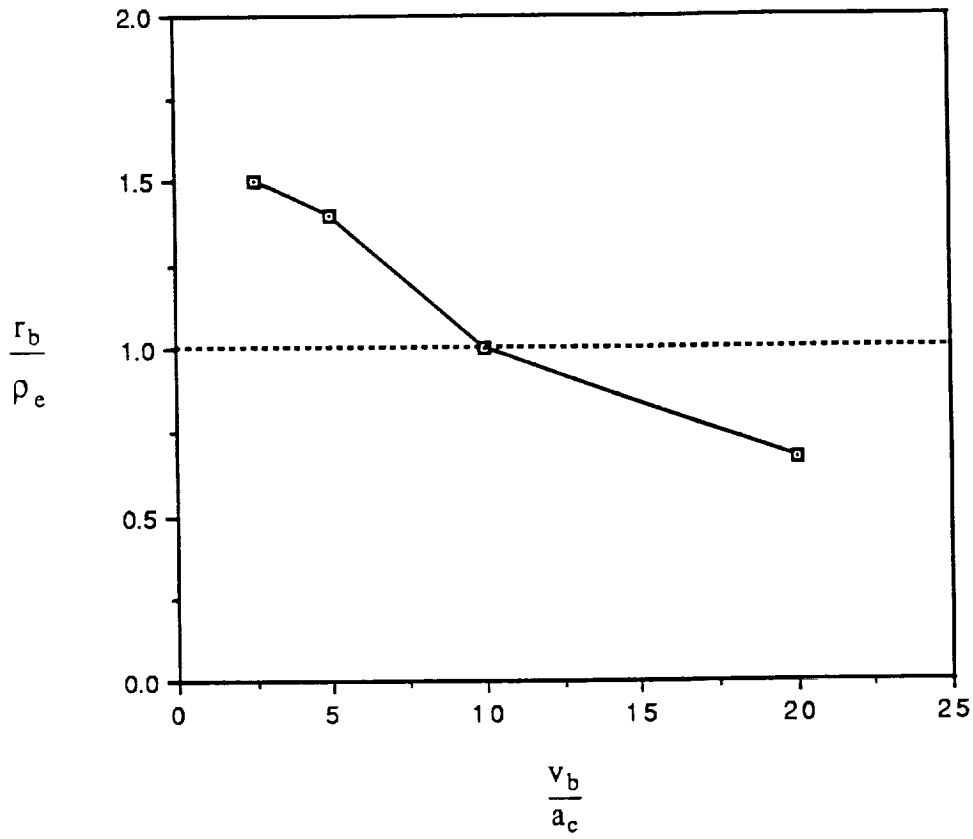

Figure 17

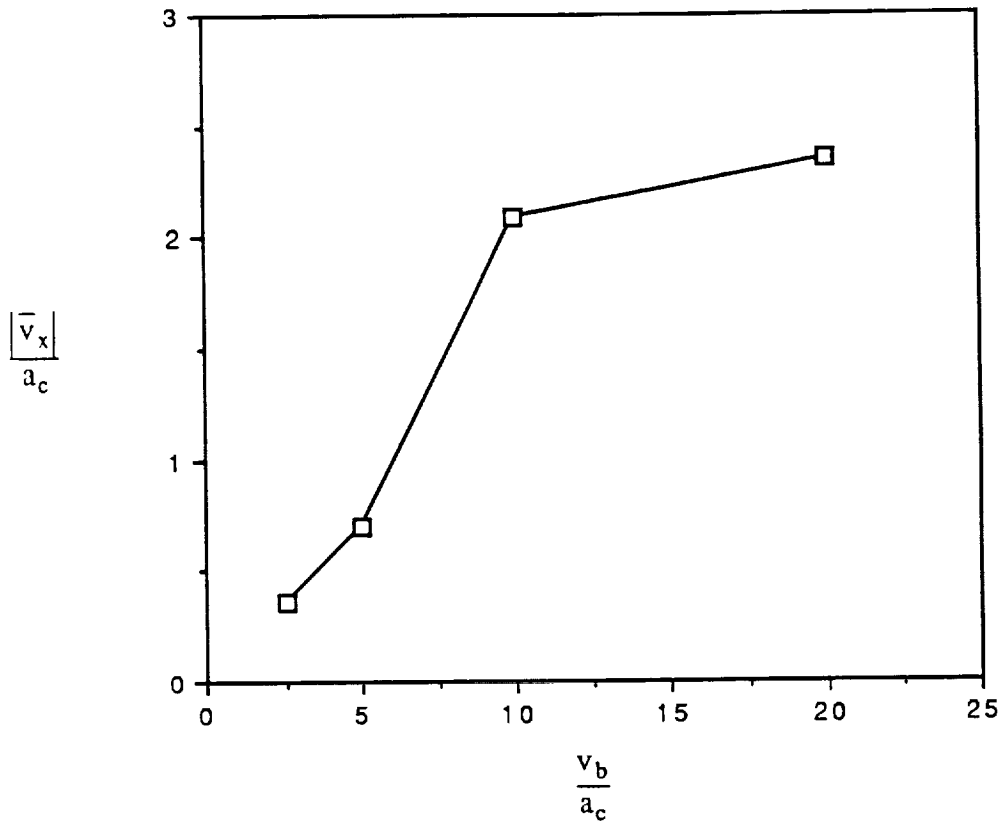

Figure 18

T-PS/17/2//26498

APPENDIX A

Spacecraft Charging Potential During Electron-Beam Injections Into Space Plasmas

Chin S. Lin
James Koga

Reprinted from
IEEE TRANSACTIONS ON PLASMA SCIENCE
Vol. 17, No. 2, April 1989

Spacecraft Charging Potential During Electron-Beam Injections Into Space Plasmas

CHIN S. LIN AND JAMES KOGA

Abstract—Injections of nonrelativistic electron beams from an infinite conductor have been simulated by using a two-dimensional electrostatic particle code to study the spacecraft charging potential. The simulations show that the conductor charging potential at the end of simulations does not vary with the beam density when the beam density exceeds four times the ambient density. The reflection coefficient, which determines a percentage of incident electrons reflected by the conductor, increases the charging potential. To charge the conductor to the beam energy, the reflection coefficient needs to be about 0.5. The results are applied to explain the spacecraft charging potential measured during the SEPAC experiments from Spacelab 1.

I. Introduction

NONRELATIVISTIC electron beams have been injected from rockets and the space shuttle to study beam propagation, instabilities, and other space plasma problems in the ionosphere [1]. At high currents, these electron beams significantly disturbed the ionosphere by producing ionization, heating, acceleration, and wave emission. Because the ambient plasma cannot neutralize the electron beam and the spacecraft, the net beam charge and the spacecraft charging are important in determining the beam propagation and expansion. Several experimental and theoretical studies have thus focused on the spacecraft charging phenomenon during the electron-beam injection [2]–[5].

At low beam current, Spacelab 2 experiments indicated that electron beams can propagate away after beam degradation and expansion [6]. However, at high beam current, spacecraft charging has limited the beam propagation. Space Experiments with Particle Accelerators (SEPAC) during the Spacelab 1 mission indicated that the electron-beam injection had charged the spacecraft to a potential as high as the beam energy, which was 5 keV [2]. Measuring energetic electrons returning to the shuttle, the SEPAC experiments suggested that some beam electrons returned due to the charging and therefore illuminated the shuttle. Furthermore, the charging potential increased linearly with the beam current for a beam current less than 100 mA, and remained constant at about the beam energy for higher beam currents. This result implies that the charging potential is independent of the beam density when the beam density is greater than a certain value.

Several simulation studies have examined the general relationship between the spacecraft charging and the electron-beam injection in the ionosphere [7]–[12]. All of these charging studies show that the positively charged spacecraft draws the ambient and beam electrons to neutralize the charging partially. Some electrons in the beam head, however, are accelerated forward and propagate away. Simulations using one-dimensional electrostatic particle codes indicate that the charging significantly prohibits the beam propagation when the beam density is greater than the ambient density [9]–[10]. Two-dimensional simulations, however, show that high-density electron beams can propagate in the plasma because the net beam charge has caused the beam to expand radially and has reduced the beam density [11], [12].

To study the spacecraft charging, we have used a two-dimensional electrostatic particle code to simulate the injection of electron beams from an infinite conductor into a plasma. The simulations have modeled the effects of electron interactions with the conductor surface by reflecting some incident electrons and absorbing the rest. The absorbed electrons represent those flowing to the surface to neutralize the charging via recombination, whereas the reflected electrons represent the backscattered and secondary electrons. By examining how the conductor potential at the end of simulations varies with the simulation parameters, we found that the conductor charging potential depends on the reflection coefficient, which is defined as the percentage of incident particles reflected by the conductor. We apply the results to explain the SEPAC measurements of spacecraft charging potentials during electron-beam injections.

II. Simulation Model

To study electron-beam injection from a conductor, we modified a 2-D particle-in-cell code DARWIN, which was originally developed at the Los Alamos National Laboratory [13]. Here we present the simulation results in the

Manuscript received August 27, 1988; revised November 11, 1988. This work was supported by the NASA Lewis Research Center through NASA Contract no. NAS8-32488 and by the Air Force Geophysical Laboratory under Contract no. F19628-85-K-004.

The authors are with the Department of Space Sciences, Southwest Research Institute, San Antonio, TX 78284.

IEEE Log Number 8926498.

electrostatic limit. Assuming that the spacecraft is much larger than the width of the injected electron beam, we consider the left boundary representing the spacecraft to be infinitely wide. Therefore, we use a periodic boundary condition for the lower boundary at $y = 0$ and the upper boundary at $y = L_y$, where L_y is the simulation length in the y direction. Fig. 1 illustrates the geometry of the simulation model.

For a perfect conductor, the electrostatic potential at $x = 0$, $\phi(x = 0, y)$ is constant. We assume that the potential is zero at the right boundary at $x = L_x$, where L_x is the simulation length in the x direction. The right-boundary condition approximates the potential at the infinity. We solve the potential in two steps. First, we determine $\phi_0 = \phi(x = 0, y)$ by integrating Poisson's equation from $x = L_x$ to $x = 0$, following a similar procedure by [11]. The integration gives $\phi_0 = 4\pi \int_0^{L_x} dx \int_{L_x}^{x} dx' \bar{\rho}(x')$, where $\bar{\rho}(x) = (1/L_y) \int_0^{L_y} dy\, \rho(x, y)$ is the charge density averaged over y. With the potential defined at the left and right boundaries, we then solve Poisson's equation again by using a finite difference method.

The simulation initializes the background ions and electrons in the system with a uniform magnetic field in the x direction. Both the background ions and electrons have Maxwellian velocity distributions with the same temperature, $T_e = T_i$, where T_e and T_i are the electron and ion temperatures, respectively. The simulation injects from the left boundary a constant flux of cold electrons with a finite beam-width along the magnetic field. At each time step, the left boundary reflects randomly a percentage of the charged particles striking the surface according to the reflection coefficient, and absorbs the rest. The code deletes the absorbed particles from the simulation. At the right boundary, the code specularly reflects all ambient ions and electrons. When the beam electrons reach the right boundary, the simulation stops.

The simulation uses a $512\Delta \times 64\Delta$ grid in the x and y directions, respectively. The grid size Δ equals the Debye length of the ambient electrons defined as $\lambda_d = a_c/\omega_{pe}$, where $a_c = (2T_e/m_e)^{1/2}$ is the thermal velocity of the ambient electrons, and ω_{pe} is the ambient electron-plasma frequency. We choose the ion-to-electron mass ratio to be 100, and $a_c = 0.001\ c$, where c is the speed of light, a unit of the simulation. We assume the electron gyrofrequency ω_{ce} to be $0.5\ \omega_{pe}$, which is close to the ionospheric value of $0.3\ \omega_{pe}$. The simulations use a time step $\Delta t = 0.05\ \omega_{pe}^{-1}$ and 262 144 particles for the background plasma. The number of injected electrons per time step per cell is $N_c(n_b/n_c)\ v_b \Delta t$, where N_c is the number of ambient electrons per cell The electron beam has a width of 8Δ, an injection velocity of $v_b = 10\ a_c$, and a zero thermal velocity. In this study, the density ratio n_b/n_0 varies from 0.5 to 10, where n_b and n_0 are the densities of the electron beam and the ambient electrons, respectively. The reflection coefficient varies from 0 for total absorption to 1 for total reflection.

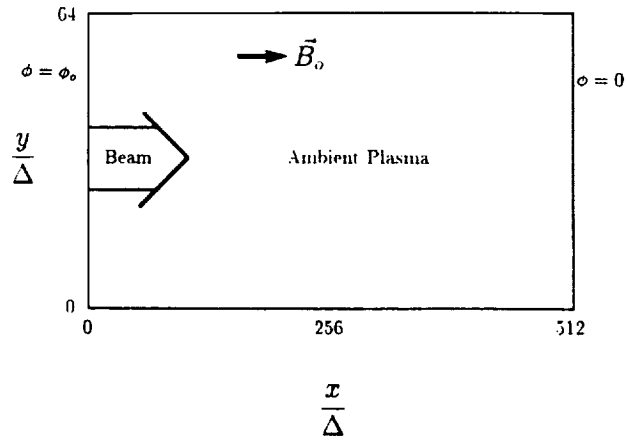

Fig. 1. Illustration of the simulation model.

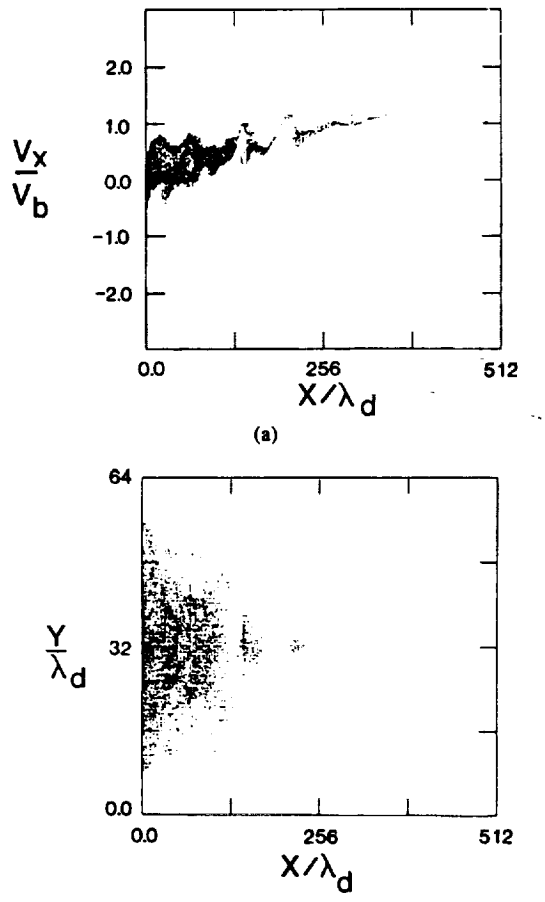

Fig. 2. Results of simulation for $n_b/n_0 = 10$ and $v_b/a_c = 10$. (a) The beam electron phase space in the $x - v_x$ plane, and (b) the positions of beam electrons in the $x - y$ plane. The position is normalized by the Debye length, and the velocity is normalized the beam velocity.

III. Simulation Results

For completeness, we briefly describe the properties of beam injection. The simulation shown in Fig. 2 has a zero reflection coefficient and a beam density ten times the ambient density. Fig. 2(a), which is a phase space plot of $v_x - x$ for beam electrons at $\omega_{pe}t = 30$, shows that the beam

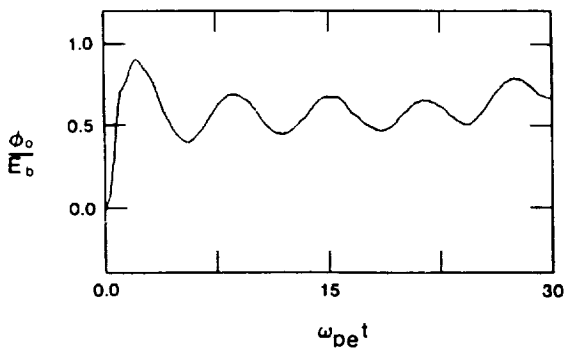

Fig. 3. Time history of the conductor potential, ϕ_0, normalized to the beam energy E_b. For this simulation, $n_b/n_0 = 10$, $v_b/a_t = 10$, and the reflection coefficient is 0.

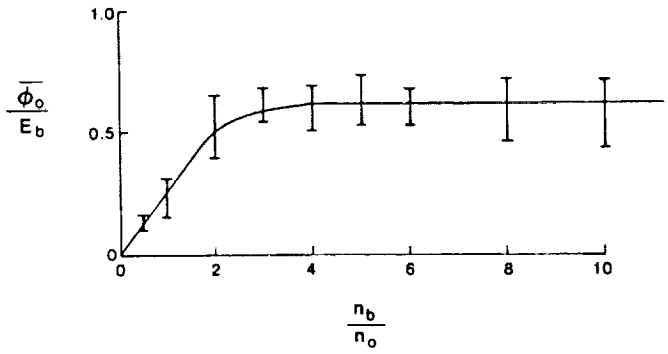

Fig. 4. Average conductor potential $\bar{\phi}_0$ normalized by E_b at $\omega_{pe}t = 30$ as a function of the density ratio n_b/n_0 for a complete absorption of particles by the conductor.

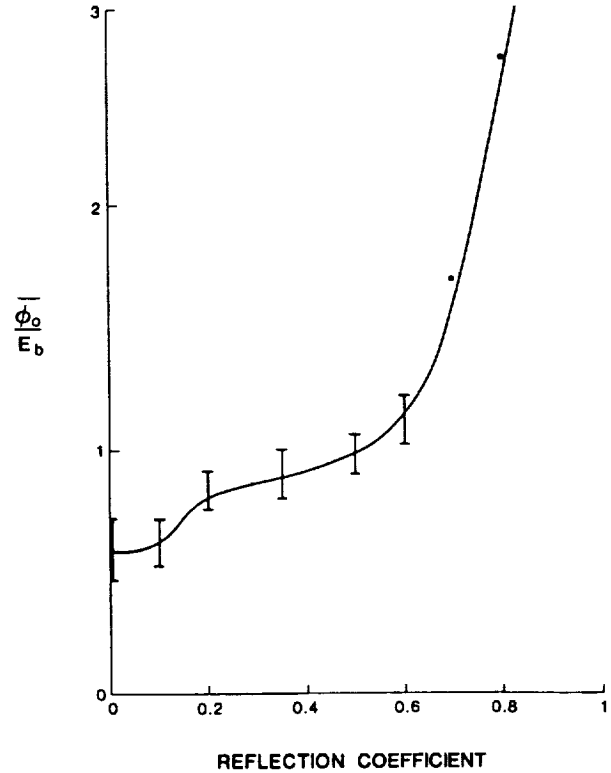

Fig. 5. Average conductor potential $\bar{\phi}_0$ normalized by E_b at $\omega_{pe}t = 30$ as a function of the reflection coefficient for $n_b/n_0 = 10$.

electron velocity decreases to zero in a very short distance from the left boundary. The distance from the left boundary to the stagnation point, where the beam velocity decreases to zero, is only 3Δ or $0.95\ v_b/\omega_{pb}$, where ω_{pb} is the plasma frequency of the beam. This distance is about twice $0.5\ v_b/\omega_{pb}$, the predicted stagnation distance for electron beams injecting into the vacuum [14]. Because the stagnation point is very close to the surface, it cannot be distinguished in Fig. 2. From the stagnation point, many beam electrons return to the left boundary and are absorbed by the conductor. However, some electrons escape from the stagnation point and form vortex patterns in the phase-space plot. The vortex wavelength is the beam-plasma instability wavelength $\lambda = 2\pi\bar{v}_b/\omega_{pb}$, where $\bar{v}_b$ is the average beam speed. Since $n_b/n_c = 10$, the beam-plasma instability has a large growth rate and reaches saturation in about $\omega_{pe}t = 15$. Because Fig. 2 shows the phase-space plot at the saturated stage of the beam-plasma instability ($\omega_{pe}t = 30$), large amplitude waves have already scattered beam electrons near the conductor surface ($x < 128\lambda_d$). Near the left boundary the average beam speed is half of its initial value v_b. A few electrons in the beam head move forward with velocities greater than the initial beam velocity ($v_x/v_b > 1$). The acceleration is caused by the repulsive force of electrons behind the beam head. Fig. 2(b), a configuration space plot of particle positions, shows that the electron beam expands in the y direction. The expansion reduces the beam density and allows some beam electrons to propagate away. These general features agree with those obtained by the previous simulations [8]–[12].

Fig. 3, which has the same parameters as Fig. 2, plots the history of the conductor potential ϕ_0 normalized by the electron-beam energy E_b. The conductor potential increases quickly to a maximum at about $0.9\ E_b$ and then oscillates around a mean value of $0.6\ E_b$ at about the ambient plasma frequency ω_{pe}. For each simulation run, we determined the mean value of the conductor potential $\bar{\phi}_0$ from the last oscillation, and examined $\bar{\phi}_0$ as a function of n_b/n_0 and the reflection coefficient. The results are shown in Figs. 4 and 5, where each data point gives $\bar{\phi}_0$, and the vertical bar represents the amplitude of potential oscillations near the end of each simulation. Fig. 4 shows that $\bar{\phi}_0$ increases linearly with n_b/n_0 for $n_b/n_0 < 4$ and remains at $0.6\ E_b$ for a n_b/n_0 greater than 4. Fig. 4 also indicates that the potential oscillation amplitude is about $0.2\ E_b$, independent of n_b/n_0. Note that the reflection coefficient for this case is zero. Therefore, we conclude that the maximum charging potential is only $0.6\ E_b$ during injections of a high-density electron beam, when the conductor absorbs all the electrons incident upon the surface.

Fig. 5 shows how the average conductor potential $\bar{\phi}_0/E_b$ varies with the reflection coefficient when $n_b/n_0 =$

10. The average conductor potential $\bar{\phi}_0$ increases from 0.6 E_b to 3 E_b when the reflection coefficient increases from 0 to 0.8. Note that $\bar{\phi}_0$ equals E_b when the reflection coefficient is about 0.5. Therefore, the conductor potential exceeds the beam energy when the conductor reflects more than half of the incident particles. When the reflection coefficient is close to 1, the conductor potential continues to increase with time and never reaches a constant value. The reason for the higher conductor potential at a larger reflection coefficient is due to a smaller number of return electrons neutralizing the positive charge on the conductor surface.

The simulations with a large reflection coefficient differ slightly from those without reflection, as shown in Figs. 2 and 3. Notably, when the conductor reflects particles, the conductor charging potential increases and electrons accumulate between the conductor boundary and the stagnation point. However, for those beam electrons that have propagated away from the stagnation point, the reflection of particles by the conductor appears to have little effect.

IV. Discussion

We have simulated the injection of a nonrelativistic electron beam from a conductor with a beam density much larger than the ambient density. Instead of totally reflecting or absorbing the incident electrons, we assume that the conductor can reflect a fraction of electrons incident on the surface and absorb the rest. Our simulations suggest that the reflection of electrons increases the charging potential. Without reflection, the maximum charging potential during injections of high-density electron beams is only about 0.6 of the beam energy. To produce a charging potential as high as the beam energy, the conductor surface needs to reflect about 50 percent of the incident electrons. Since the shuttle was charged to the beam energy during the SEPAC experiments, we conclude that the simulation would agree with the SEPAC results if the conductor reflects about half of the incident electrons.

Besides the reflection coefficient, the conductor size relative to the beam radius is another parameter affecting charging potential. Unfortunately, our simulation model cannot rigorously examine the effect of this parameter because we have assumed an infinite conductor surface. The simulation results presented here are valid within the limit that the conductor surface is much larger than the beam radius. For the SEPAC experiments, the electron-beam radius is 10 cm, and the scale length of the shuttle payload bay is about 10-m long, about 100 times larger than the beam radius. Therefore, the assumption of an infinite conductor surface would be justified.

Another approach to simulate beam injection has been to use an isolated system [12], which has an advantage of examining beam injection from a small spacecraft. Reference [12] found a charging potential larger than the beam energy when the spacecraft is only four times the beam radius and the reflection coefficient is zero. The reason for the higher charging potential is that only a fraction of the returning electrons will strike the conductor surface. The reminder will propagate past the spacecraft and thus not contribute to neutralization. However, when the spacecraft size is 16 times the beam radius, [12] obtained a charging potential of about 0.3 E_b, about half of the charging potential given in Fig. 4 for the zero reflection coefficient. Therefore, the present results are consistent with those of the isolated system when the conductor system length is much larger than the beam radius.

The purpose of this study is to point out the importance of the reflection of electrons on the charging potential. However, to compare the simulation results with the experimental results quantitatively, the simulation model will need to include more sophisticated reflection processes. The reflected electrons in the simulations represent backscattered and secondary electrons. Our simulation model simply reflects electrons from the surface regardless of the velocity. However, the backscattering and secondary production processes should depend on the incident velocity. Future studies will include more realistically the reflection processes.

Acknowledgment

The authors would like to thank H. Okuda, J. S. Wagner, and D. Winske for useful discussions.

References

[1] B. Grandal, *Artificial Particle Beams in Space Plasma Studies*. New York: Plenum, 1982.
[2] S. Sasaki, N. Kawashima, K. Kuriki, M. Yanagisawa, and T. Obayashi, "Vehicle charging observed in SEPAC Spacelab-1 experiment," *J. Spacecr. Rockets*, vol. 23, no. 2, p. 129, 1986.
[3] S. Sasaki *et al.*, "Neutralization of beam-emitting spacecraft by plasma injection," *J. Spacecr. Rockets*, vol. 24, no. 3, p. 227, 1987.
[4] I. Katz, A. Jongeward, D. E. Parks, D. L. Reasoner, and C. K. Purvis, "Energy broadening due to space-charge oscillations in high-current electron beams," *Geophys. Res. Lett.*, vol. 13, no. 1, p. 64, 1986.
[5] J. A. Marshall, C. S. Lin, J. L. Burch, T. Obayashi, and C. Beghin, "Spacelab 1 experiments on interactions of an energetic electron beam with neutral gas," *J. Spacecr. Rockets*, vol. 25, no. 5, p. 361, 1988.
[6] D. A. Gurnett *et al.*, "Whistler-mode radiation from the Spacelab-2 electron beam," *Geophys. Res. Lett.*, vol. 13, no. 3, p. 225, 1986.
[7] Y. Omura and H. Matsumoto, "Computer simulations of beam injection experiments for SEPAC/Spacelab 1 mission," *Radio Sci.*, vol. 19, no. 2, p. 496, 1984.
[8] P. L. Pritchett and R. M. Winglee, "The plasma environment during particle beam injection into space plasmas, I: Electron beams," *J. Geophys. Res.*, vol. 92, no. A7, p. 7673, 1987.
[9] R. M. Winglee and P. L. Pritchett, "Space-charge effects during the injection of dense electron beams into space plasmas," *J. Geophys. Res.*, vol. 92, no. A6, p. 6114, 1987.
[10] H. Okuda and J. R. Kan, "Injection of an electron beam into a plasma and spacecraft charging," *Phys. Fluids*, vol. 30, no. 1, p. 209, 1987.
[11] H. Okuda and J. Berchem, "Injection and propagation of a nonrelativistic electron beam and spacecraft charging," *J. Geophys. Res.*, vol. 93, no. A1, p. 175, 1988.
[12] R. M. Winglee and P. L. Pritchett, "Comparative study of cross-field and field-aligned electron beams in active experiments," *J. Geophys. Res.*, vol. 93, no. A6, p. 5823, 1988.
[13] C. W. Nielson and H. R. Lewis, "Particle simulation techniques in the nonradiative limit," *Methods Comput. Phys.*, vol. 16, p. 367, 1976.
[14] D. E. Parks, A. R. Wilson, and I. Katz, "Monode plasma sheath dynamics," *IEEE Trans. Nucl. Sci.*, vol. NS-22, no. 6, p. 2368, 1975.

Chin S. Lin was born in Taiwan on July 10, 1947. He received the B.S. degree in physics from the National Taiwan University in 1969, and the Ph.D. degree in physics from the University of Washington at Seattle in 1975.

He first worked at the NASA/Goddard Space Flight Center as a National Research Council Research Associate in 1975, and then joined the Geophysics Program at the University of Washington as a Research Assistant Professor in 1976. From 1979 to 1981 he was at the Institute for Physical Sciences and Technology at the University of Maryland as a Visiting Assistant Professor. Since 1981 he has been at the Southwest Research Institute, San Antonio, TX, where he is currently the Manager of the Plasma Physics Section in the Instrumentation and Space Research Division. His research interests include space plasma physics, auroral phenomena, plasma simulations, and parallel computation.

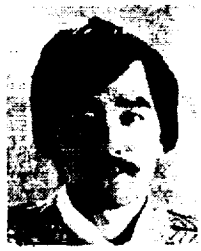

James Koga was born in Stockton, CA, in 1959. He received the B.S. degree in physics from the Massachusetts Institute of Technology, Cambridge, MA, in 1981, and the M.A. degree in plasma physics from the University of Texas at Austin in 1985. He is currently working towards the Ph.D. degree in plasma physics at the University of Texas at Austin.

From 1984 to 1985 he was a Programmer/Analyst at Zycor, Inc., in Austin, TX. Since 1985 he has been a Research Scientist in the Department of Space Sciences at the Southwest Research Institute in San Antonio. His current interests include plasma simulation and parallel processing techniques.

APPENDIX B

Further Studies of ELF Oscillations During Electron-Beam Firings on Spacelab 1

Jill A. Marshall
Chin S. Lin
James L. Burch

Reprinted from
IEEE TRANSACTIONS ON PLASMA SCIENCE
Vol. 18, No. 1, February 1990

Technical Notes

Further Studies of ELF Oscillations During Electron-Beam Firings on Spacelab 1

JILL A. MARSHALL, CHIN S. LIN, AND JAMES L. BURCH

Abstract—**Injections from an electron beam that comprised part of the PICPAB (Phenomena Induced by Charged Particle Beams) experiment were observed by the SEPAC (Space Experiments with Particle Accelerators) plasma diagnostic package. In particular, extremely low-frequency (ELF) oscillations from 150 to 200 Hz were seen in the SEPAC Langmuir probe current. The strongest oscillations occurred when the ambient pressure was augmented by neutral gas releases from the SEPAC plasma accelerator (the Magnetoplasma Dynamic Arcjet, or MPD).**

I. Introduction

Extremely low-frequency (ELF) oscillations have been reported in the return current to the SEPAC (Space Experiments with Particle Accelerators) diagnostic probes during firings of an electron beam on Spacelab 1 by Cai *et al.* [1]. Those authors found a correlation between the amplitude of the ELF oscillations and the charge-up potential of the orbiter, which led them to conclude that these oscillations are expressions of fluctuations in the return current to the spacecraft. They proposed that the oscillations may be electrostatic ion-cyclotron waves generated close to the Shuttle, possibly in a co-moving plasma cloud.

In this technical note we report similar observations with the same diagnostic package during firings of the electron beam from the PICPAB (Phenomena Induced by Charged Particle Beams) experiment [2]. In all the cases studied here, the 8-keV PICPAB beam was fired at a current of 100 mA for a 20-ms pulse every ~266 ms. Some of these firings occurred at times when the neutral pressure near the orbiter had been elevated above 7×10^{-5} by a release of neutral argon from one of the SEPAC plasma accelerators (the Magnetoplasma Dynamic Arcjet or MPD).

II. Results

The PICPAB beam firings were recorded four times a second by increases in the current attracted to the SEPAC Langmuir probe. This current was sampled once every ms, making it just possible to detect oscillations in the ELF range. Fig. 1, for example, shows one Langmuir current pulse (from Dec. 7, 1983, 2:24:31.580 to 2:24:31.620 UT) plotted versus time. The ELF oscillations are clearly evident for 20 ms during the beam-firing at 2:24:31.585 UT. In the 21 cases of firings, such as this one, which were coincident with neutral gas releases from the SEPAC MPD, the Langmuir probe current shows very regular oscillations; these data were analyzed, yielding frequencies between 167 and 225 Hz, with an average of 185 Hz. Oscillations are also seen during firings into the ambient plasma alone; however, they are much more irregular and lower in amplitude than those shown in Fig. 1.

To more accurately identify the peak frequency of the oscillations, the Langmuir current data during the firings were Fourier transformed. Since the PICPAB beam was fired for only 20 ms, there are only 20 contiguous samples for the FFT, limiting the accuracy of the resulting frequencies to ±45 Hz and increasing the background noise. The Fourier-transformed data indicate that the Langmuir current oscillates at frequencies ranging from 50–400 Hz, with the highest amplitude frequencies between 150–200 Hz.

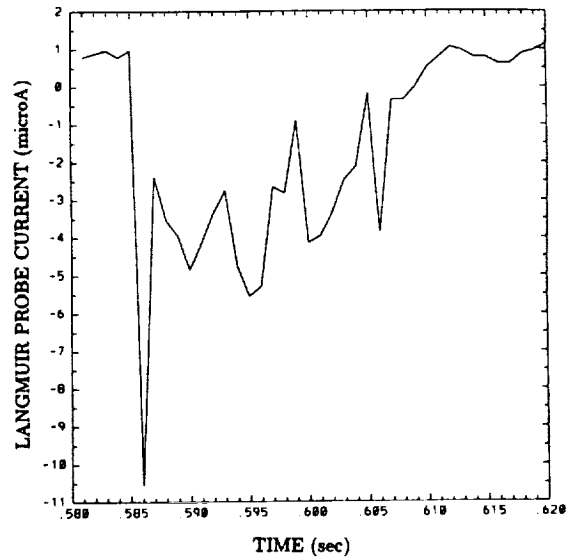

Fig. 1. SEPAC Langmuir current data from Dec. 7, 1983 (Day 341) 2:24:31.580–31.620 UT (after the neutral gas is released).

The above-mentioned variation in the amplitude of the ELF oscillations with changes in neutral pressure is documented in Fig. 2. The amplitude of the oscillations is plotted versus frequency, both for times when the ambient neutral pressure was enhanced by a gas release from the SEPAC MPD and for times when the pressure was at the background level. The circles represent data taken during releases when the ambient neutral pressure (as measured by the SEPAC ionization gauge) increased to 7×10^{-5} torr. The stars represent data taken when the neutral pressure remained below 10^{-5} torr. This figure shows that the amplitude of the oscillations tends to increase with neutral pressure. This correlation led us to investigate a density-gradient drift wave as an alternate source for the oscillation; however, the frequencies predicted for such a wave with the given beam-density distribution are higher than the observed frequencies.

In some cases of firings coincident with neutral gas releases, the SEPAC floating probes also recorded the beam firings, indicating a potential difference between the probe sensors (grounded to the spacecraft) and the surrounding plasma. The amplitude of the oscillations was found to increase with the potential difference. This dependence of the ELF activity on spacecraft potential confirms the results of [1] related to Langmuir current oscillations during firings of the SEPAC electron beam. It seems to support the interpretation that the ELF oscillations represent fluctuations in the return current to the orbiter.

III. Discussion and Conclusions

ELF activity during firings of the SEPAC electron beam has been suggested by [1] to be the potential-driven electrostatic ion-cyclotron oscillation, which is the result of ions gyrating in response to

Manuscript received August 15, 1989; revised October 2, 1989.

The authors are with the Southwest Research Institute, 6220 Culebra Road, Postal Drawer 28510, San Antonio, TX 78284.

IEEE Log Number 8932749.

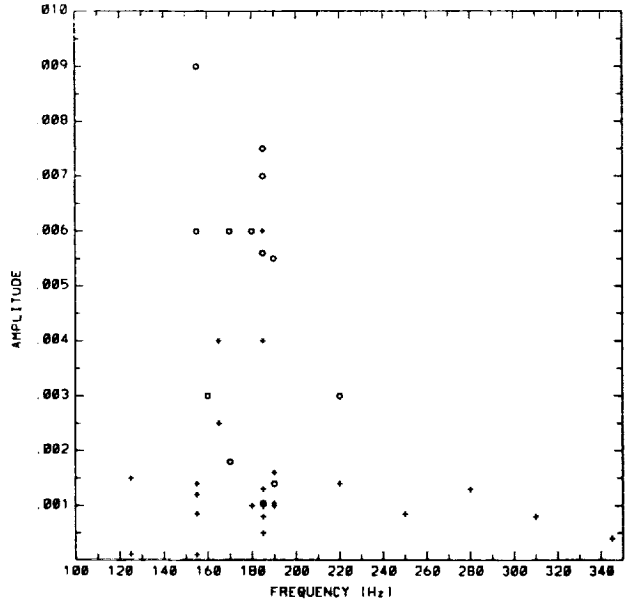

Fig. 2. Scatter plot of amplitude versus frequency for the peak frequencies of the FFT spectra from a wide sample of Langmuir current data during PICPAB beam-firings. Circles represent firings when the ambient neutral density is enhanced by an argon release from the SEPAC MPD; stars represent firings when there is no added neutral density.

fluctuations in the potential on an electrode immersed in a plasma. In this case, the orbiter itself acts as the electrode, and a positive potential is induced when the electron gun is fired. The mechanism is discussed more extensively in [3].

Such a mechanism should operate *a priori* at the ion-cyclotron frequency of common ionospheric ions in a 0.3-G magnetic field. This would be 456 Hz for H^+, ~30 Hz for N^+ or O^+, and ~11 Hz for A^+. The 150–200-Hz frequency observed in these data cannot be identified as the cyclotron frequency for any ambient ion species; however, the presence of a potential gradient perpendicular to a magnetic field results in an oscillatory motion in addition to the cyclotron motion, as described in [4]. In such cases the wave frequency differs from the cyclotron frequency by a correction term which depends on the radial gradient of the electric field. A potential gradient can be seen in the SEPAC floating probe data (see [2]); however, the potential was only measured at three points and data are only available in a very limited number of cases; thus we could not estimate the electric-field gradient and calculate the correction to the cyclotron frequency. It is also possible that the observed frequencies could represent a H^+–O^+ hybrid-cyclotron frequency (116 Hz) (see [5]). The relative motion between the ionized gas and the spacecraft might Doppler-shift the multi-ion hybrid resonance frequency to the observed frequencies.

References

[1] D. Cai *et al.*, "ELF oscillations associated with electron beam injections from the space shuttle," *J. Geophys. Res.*, vol. 92, p. 12451, 1987.

[2] J. A. Marshall, C. S. Lin, J. L. Burch, T. Obayashi, and C. Beghin, "Spacelab 1 experiments on interactions of an energetic electron beam with neutral gas," *J. Spacecr. Rockets*, vol. 25, p. 361, 1988.

[3] N. Sato and R. Hatakeyama, "A mechanism for potential-driven electrostatic ion-cyclotron oscillations in a plasma," *J. Phys. Soc. Japan.*, vol. 54, p. 1661, 1985.

[4] N. Sato, "Some details of potential-driven ion-cyclotron oscillations in a magnetized plasma column," in *Proc. Workshop Current-Driven Electrostatic Ion-Cyclotron Instability* (Innsbruck, Austria), July 9–10, 1987. Singapore: World Science, 1988, p. 29.

[5] S. J. Buchsbaum, "Resonance in a plasma with two ion species," *Phys. Fluids*, vol. 3, p. 418, 1960.